

University of Alberta

Corrosion Protection of copper by self-assembled monolayer

by



Chao Yang

A thesis submitted to the Faculty of Graduate Studies and Research in partial fulfillment
of the requirements for the degree of *Master of Science*

in

Materials Engineering

Department of Chemical and Materials Engineering

Edmonton, Alberta, Canada

Fall, 2002



National Library
of Canada

Acquisitions and
Bibliographic Services

395 Wellington Street
Ottawa ON K1A 0N4
Canada

Bibliothèque nationale
du Canada

Acquisitions et
services bibliographiques

395, rue Wellington
Ottawa ON K1A 0N4
Canada

Your file Votre référence

Our file Notre référence

The author has granted a non-exclusive licence allowing the National Library of Canada to reproduce, loan, distribute or sell copies of this thesis in microform, paper or electronic formats.

The author retains ownership of the copyright in this thesis. Neither the thesis nor substantial extracts from it may be printed or otherwise reproduced without the author's permission.

L'auteur a accordé une licence non exclusive permettant à la Bibliothèque nationale du Canada de reproduire, prêter, distribuer ou vendre des copies de cette thèse sous la forme de microfiche/film, de reproduction sur papier ou sur format électronique.

L'auteur conserve la propriété du droit d'auteur qui protège cette thèse. Ni la thèse ni des extraits substantiels de celle-ci ne doivent être imprimés ou autrement reproduits sans son autorisation.

0-612-81503-X

University of Alberta
Library Release Form

Name of Author: Chao Yang


Title of Thesis: Corrosion Protection of copper by self-assembled monolayer

Degree: Master of Science

Year this Degree Granted: 2002

Permission is hereby granted to the University of Alberta Library to reproduce single copies of this thesis and to lend or sell such copies for private, scholarly or scientific research purposes only.

The author reserves all other publication and other rights in association with the copyright in the thesis, and except as herein before provided, neither the thesis nor any substantial portion thereof may be printed or otherwise reproduced in any material form whatever without the author's prior written permission.



Chao Yang

Department of chemical and materials Engineering
University of Alberta
Edmonton, AB, Canada, T6G 2G6

July 30, 2002

University of Alberta

Faculty of Graduate Studies and Research

The undersigned certify that they have read, and recommend to the Faculty of Graduate Studies and Research for acceptance, a thesis entitled *Corrosion Protection of copper by self-assembled monolayer* submitted by *Chao Yang* in partial fulfillment of the requirements for the degree of *Master of Science* in Materials Engineering.



Dr. Jingli Luo, Supervisor



Dr. Daniel Y. Kwok, Examining Committee Member



Dr. Qi Liu, Examining Committee Member

Date:

July 24, 2002

Abstract

The self-assembled monolayers (SAMs) of three n-alkanethiols, 1-octadecanethiol (C18SH), 1-dodecanethiol (C12SH), and 1-hexanethiol (C6SH), were formed on the fresh copper surface which was cathodically reduced in 1 M HClO₄, followed by etching in 7 M HNO₃. The effect of the alkanethiol SAMs on the anodic dissolution of the copper substrate was investigated by the cyclic voltammetry and Fourier transform infrared spectrometer (FTIR). The voltammetric results show that the SAMs are capable of inhibiting the oxidation of copper from Cu(0) to Cu(I), but exhibit little resistance to retard the oxidation at more anodic potentials. FTIR measurements confirm that the alkanethiol SAMs are desorbed electrochemically from the copper surface at the high potential. The corrosion protection abilities of three SAMs were evaluated in 0.2 M NaCl by polarization techniques and in 0.2 M NaCl, 0.2 M HCl and 0.2 M H₂SO₄ by using electrochemical impedance spectroscopy (EIS) method. It is found that the alkanethiol SAMs have stronger inhibition on the cathodic reaction than the anodic reaction, and the longer hydrocarbon chains are more favorable for their protection ability against copper corrosion. The SAMs act as the hydrophobic monolayers, which block effectively the transport of reactants and inhibit the corrosion reactions at the copper substrate. A general equivalent circuit for the SAMs-coated electrode was proposed, by means of which the impedance behavior of the electrodes was interpreted and the electrochemical parameters

were acquired. In addition, the quality of SAMs and development of defects in SAMs were evaluated based on the circuit. The dependence of the electrode capacitance on the applied potential was used to determine the stability of SAMs at the applied potential. The Electrochemical Noise (EN) measurements provide a good method to in situ monitor the corrosion process of the copper surface modified by the Alkanethiol SAMs and the results showed the copper substrate of copper electrodes suffered pitting because the defective sites were attacked by the chloride ions. The defects of SAMs were detected through measuring the electron work function (EWF) of the electrode sample surfaces by means of Scanning Kelvin Probe.

TABLE OF CONTENTS

Chapter 1. Introduction	1
Chapter 2 Literature Review	3
2.1 Introduction	3
2.2 Some typical SAMs model systems	4
2.2.1 Monolayers of organosulfur on Metals and Semiconductor substrate... 4	
2.2.2 Monolayers of organosilicon derivatives	7
2.2.3 Monolayers of fatty acid	8
2.3 Sample Preparation.....	8
2.3.1 Substrate preparation	8
2.3.2 Assembly process.....	10
2.4 Characterization Techniques	12
2.4.1 Spectroscopy methods	12
2.4.2 Microscopy methods.....	15
2.4.3 Other methods.....	16
2.5 Structure.....	18
2.6 Kinetic of adsorption.....	22
2.7 Stability of SAMs.....	23
2.7.1 Thermal stability of SAMs.....	23
2.7.2 Stability of SAMs in air	25
2.7.3 Stability of SAMs in corrosive solution.....	29
2.8 Applications and future work	30
2.8.1 Intermolecular interactions and surface engineering in SAMs.....	30
2.8.2 Corrosion protection by SAMs	32
2.9 Summary	33
2.10 Reference.....	33
Chapter 3 Experimental Section	42
3.1 Chemicals	42
3.2 Preparation of Copper Electrodes.....	42
3.3 Monolayer Self-Assembly	42
3.4 Electrochemical Measurements	43
3.5 FTIR measurements.....	45

3.6 Scanning Kelvin Probe Experiments.....	45
Chapter 4. Results and Discussion	47
4.1 Voltammetric Characterization	47
4.2 FTIR Characterization	50
4.3 Polarization Curves.....	51
4.4 EIS Results	54
4.4.1 EIS Evaluation on SAMs in corrosive solutions.....	54
4.4.2 EIS Evaluation on Formation Process of C12SH SAMs.....	60
4.4.3 The Destruction of C12SH SAMs in NaCl.....	61
4.4.4 Stability of Alkanethiol SAMs as a Function of Applied Potential.....	62
4.5 Measurements of Electrochemical Noise (EI).....	64
4.6 Scanning Kelvin Probe (SPK)	66
4.7 Summaries.....	67
CHAPTER 5. CONCLUSIONS AND FUTURE WORK	
.....	96
5.1. Conclusions	96
5.2. Future work	96

LIST OF FIGURES

CHAPTER 2.

Figure 2-1.	A schematic graph of Self-assembled monolayers
Figure 2-2.	A schematic graph of organosilicon monolayer at substrate surface
Figure 2-3.	A schematic illustration of fatty acid monolayer structure
Figure 2-4.	Assembly procedure of adsorption from solution
Figure 2.5.	Schematic diagram of an all-trans chain orientation in an n-alkanethiols monolayer on gold surface
Figure 2.6.	Mechanism of of corrosion of SAM with hydrophobic endgroup in halide solution
Figure 2.7.	Mechanism of corrosion of SAM with hydrophilic endgroup in halide solution

CHAPTER 4.

- Figure 4-1. Cyclic voltammograms of naked copper in 0.2 M NaCl solution.....
- Figure 4-2. Cyclic voltammograms of naked copper in 0.2 M NaCl solution.....
- Figure 4-3. Cyclic voltammograms for C18SH-covered copper electrodes in 0.2 M NaCl solutions.....
- Figure 4-4. Cyclic voltammograms for C18SH-covered copper electrodes in 0.2 M NaCl solutions.....
- Figure 4-5. Cyclic voltammograms for C12SH-covered copper electrodes in 0.2 M NaCl solution.
- Figure 4-6. Cyclic voltammograms for C6SH-covered copper electrodes in 0.2 M NaCl.....
- Figure 4-7. FTIR reflection spectra for the copper electrode coated by C18SH SAMs in 0.2 M NaCl solution before the potential scan (A) and at anodic potentials of 0.014 V (B), 0.30 V(C) and 0.85 V (D).....
- Figure 4-8. Polarization curves for the naked copper electrode and the SAMs-coated copper electrodes in 0.2 M NaCl solution
- Figure 4-9. Nyquist impedance spectra for the naked (A) and alkanethiol-SAMs-covered (B) copper electrodes in 0.2 M NaCl solutions at the open-circuit potentials. Formation times of SAMs are 4h.
Symbols: measured data; solid line: fitted curve
- Figure 4-10. Nyquist impedance spectra for the naked (A) and alkanethiol-SAMs-covered (B) copper electrodes in 0.2 M HCl solutions at the open-circuit potentials. Self-assembling times of alkanethiol monolayers at copper are 4h
Symbols: measured data; solid line: fitted curve
- Figure 4-11. Nyquist impedance spectra for the copper electrodes of naked (A) and covered by alkanethiol SAMs in 0.2 M H₂SO₄ solutions at the open-circuit potentials. Alkanethiol monolayers were self-assembled for 4h
Symbols: measured data; solid line: fitted curve

- Figure 4-12. Equivalent circuits for the impedance spectra composed of a high frequency capacitive loop and a Warburg impedance
- Figure 4-13. The equivalent circuit of a defect-free SAM (A) and the Nyquist impedance plot for the electrode coated by the defect-free SAMs (B).....
- Figure 4-14. Equivalent circuits for the electrode covered by the SAMs with defects under varying conditions.....
- Figure 4-15. Effect of self-assembling times for C12SH SAMs at copper on their impedance behavior. Impedance measurements were carried out in 0.2 M NaCl solution at the open-circuit potentials.....
- Figure 4-16. The dependence of Y_0 and n for Q_{sam} on the formation time of C12SH SAMs
- Figure 4-17. Variation of Nyquist impedance spectra for the C12SH-SAMs-coated copper electrode with immersion time in 0.2 M NaCl solution. C12SH monolayers were self-assembled.
- Figure 4-18. Variation of Y_0 and n for Q_{sam} with the immersion time in 0.2 M NaCl. Before test the copper electrode was immersed in 1 mM C12SH ethanol solution for 4h.....
- Figure 4-19. Values of C as a function of applied potentials for the copper electrodes coated by the C12SH SAMs forming after various immersion times in 1mM C12SH ethanol solution.
- Figure 4-20. Electrochemical Noise for C18SH SAMs-covered copper electrode in 0.2 M HCl solution at the open-circuit potential (first 2000 seconds).....
- Figure 4-21. Electrochemical Noise for C18SH SAMs-covered copper electrode in 0.2 M HCl solution at the open-circuit potential (2000 – 4000 seconds)...
- Figure 4-22. Electrochemical Noise for C18SH SAMs-covered copper electrode in 0.2 M HCl solution at the open-circuit potential (4000-6000 seconds).....
- Figure 4-23. Electron work functions of copper modified by PhCH₂SH (A) and C12SH (B) SAMs.

NOTATION

Roman Letters

A	Ampere
A	Area
C	Capacity
C	Coulomb (unit of charge), $1C=1A/s$
c	Centi (10^{-2})
c	Concentration
d	Thickness
E	Energy; electric field
E_{oc}	Open Circuit potential
e^-	Electron (charge)
F	Faraday constant (96484.5 C/equi.)
I	Current Density (A/cm^2)
m	Meter
Q	Charge, Q/A charge per unit area
T	Absolute temperature ($t + 273.15$) in Kelvin (K)
t	Time; temperature in $^{\circ}C$
V	Voltage, potential difference
Z	Impedance

Greek Letters

ϵ_0	Permittivity of free space
ρ	Density

Subscripts and Superscripts

A	Acceptor
a	Anodic
- b	Bulk
c	Cathodic
e	Electronic; equilibrium
H	Helmholtz
n	Electron
sc	Space charge region (of semiconductor)
SAM	Self-assembled monolayer

Chapter 1. Introduction

The spontaneous self-assembly of amphiphiles on solid substrates is becoming increasingly a specific technique to prepare compact monolayers with controlled thickness and structure. Over the past 20 years, self-assembled monolayers (SAMs) and multilayers have been extensively studied for their potential application as new materials.

Areas of possible application of SAMs range from surface modification such as wettability control and lubrication to sensors and surface devices. Besides, SAMs also provide opportunities to enhance the fundamental understanding of self-organization and structure-property relationships. Furthermore, SAMs are excellent systems to investigate interactions at interfaces, which include intermolecular, molecular-substrates and molecular-solvent interaction.

Copper and its alloys are widely used in chemical and electronics industries due to their high thermal and electrical conductivities, low cost and low corrosion susceptibility. From the viewpoint of practical application, it is valuable to prepare alkanethiol SAMs on copper. Therefore, we focus our studies on the preparation and characterization of SAMs of octadecanethiol, dodecanethiol and hexanethiol on copper substrates.

There are three main objectives of this study.

1. To characterize the potential-induced defects in SAMs.

2. To investigate the corrosion protection ability of SAMs on copper in electrolyte solution.
3. To compare the corrosion protection ability of SAMs of n-alkanethiols with different hydrocarbon chains.

Chapter 2 introduces a brief review on self-assembled monolayer characteristics and presents relevant laboratory studies on SAMs. Chapter 3 presents the experimental conditions, including sample preparation and the setup of experiments. Chapter 4 covers the results and discussion. Finally, conclusions are made in Chapter 5 along with recommendations for further work.

Chapter 2 Literature Review

2.1 Introduction

This chapter presents an overview of general characteristics and structure of self-assembled monolayers (SAMs) system.

Self-assembly is defined as the spontaneous formation of complex molecular aggregate structures.^[1-4] SAMs are close-packed, ordered molecular assemblies that are spontaneously formed on the substrate surface by the adsorption of amphifunctional molecules, one part of which has a specific strong affinity for the surface and the other part has very weak affinity or none.^[5] The interactions between molecules and substrate, generally a chemical bond, result in a pinning of the headgroup to a specific site on the substrate surface. A schematic graph of SAMs is shown in Figure 2.1, which shows the constituents of interactions within SAMs.

In nature, SAMs are different from the Langmuir-Blodgett film. Langmuir-Blodgett techniques involve the transfer of a surfactant film assembled at an air-liquid interface to a solid substrate, and the components are typically weakly bound to the substrate surface. However, SAMs are based on the spontaneous chemical adsorption of the film compounds from a gas phase or a solution directly onto the substrates, and the bonding of monolayer molecules to the substrate surface is much stronger than that in the Langmuir-Blodgett film.

In the past two decades, SAMs have been extensively investigated on a microscopic level by developing characterization techniques. The most attractive features of SAMs come from their utilization in surface engineering such as semiconductor surface patterning, wettability control, lubrication, and corrosion protection. Transducer technology, for optical, piezoelectric and other forms of chemical sensors, is another example of SAMs application.

2.2 *Some typical SAMs model systems*

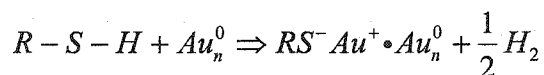
In recent years, the field of SAMs has experienced tremendous growth in both the depth of characterization and sophistication.^[1] SAMs are manufacturable and attractive for building surface engineering. A brief introduction of several extensively studied systems is presented in this part.

2.2.1 Monolayers of organosulfur on Metals and Semiconductor substrate

The phenomenon of spontaneous adsorption of alkanethiolates on gold was first discovered by Nuzzo and Allara.^[6] This intriguing behavior has since been reexamined in numerous following studies. To date, it has been established that surface-active organosulfur derivatives have a strong affinity to many metals and metal sulfides due to the formation of multiple bonds with surface metal clusters. Besides gold, it has been found that organosulfur compounds could

coordinate strongly to silver,^[7] copper,^[7-9] platinum, mercury,^[10] iron,^[11] γ -Fe₂O₃ particles,^[12] SiO₂, GaAs,^[13, 14] and InP.^[15]

Although gold is generally considered as a chemically inert element and resists atmospheric contamination, it has a strong specific interaction with organosulfur compounds ranging from linear chain alkanethiols to complex molecules such as thiol-bearing porphyrins^[16] and C₆₀.^[17] In fact, the monolayers of alkanethiolates on gold are probably the most studied system in SAMs to date. In the alkanethiol case, the self-assembly process is believed to involve an oxidative addition of an S-H bond to the gold surface, followed by a reductive elimination of the hydrogen:

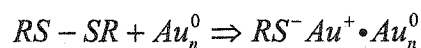


While some debate still remain on the reaction mechanism, one conclusion has been reached unanimously, i.e. the chemisorbed species on gold is a thiolate.^[18]

On the basis of thermodynamics, the overall free energy change $\Delta G^\circ_{\text{adsorption}}$ is about -21 kJ mol^{-1} , which means that the reaction is exothermic and could spontaneously happen. Schlenoff reported a similar value, $-23.1 \text{ kJ mol}^{-1}$, by using electrochemical data.^[19] The adsorption bond energy was estimated at about $30 \text{ to } 35 \text{ kcal mol}^{-1}$ for long-chain alkanethiols on gold, larger than the 28 kcal mol^{-1} for short chain adsorbates on gold.^[20] The enhanced interchain van der Waals (VDW) attraction energy further stabilizes the products. The lateral interaction of the alkyl chains enhances the stability of the monolayer by

approximate 0.8 kcal per mole of CH₂ groups, which is less than the van der Waals interaction energy of a crystalline hydrocarbon chain, i.e. 1.3 kcal per mole of CH₂. However, this value is slightly larger than the group constituent heats of vaporization or fusion for normal paraffin (0.6 kcal per mole of CH₂). Therefore, long-chain alkanethiols form a high-density packing, crystalline or liquid-crystalline monolayer on gold.^[21, 22]

On the other hand, in the formation of SAMs from dialkyl disulfide, the mechanism probably involves a simple cleavage of disulfide (S-S) bond followed by immediate oxidation addition to the gold surface.



Based on thermodynamics, the free energy change is about -101 kJ mol⁻¹, approximately twice as favorable as that of alkanethiol adsorption. The structures of SAMs formed by chemisorption of dialkyl disulfides and corresponding alkanethiols are indistinguishable.^[23] Although the formation rates of SAMs from alkanethiols as well as dialkyl disulfides were similar, the replacement rate of molecules on SAMs formed by alkanethiol were much faster than those formed by dialkyl disulfides. The difference in replacement rate might arise from the larger bulk of dialkyl disulfide. However, the contact angles of SAMs formed from alkanethiols were lower than those formed from dialkyl disulfides, which indicated that the dialkyl disulfides are kinetically slow to complete the monolayers.^[24]

Copper and silver are more reactive to alkanethiols and more sensitive to attributes of the alkanethiol than gold. The mechanism of formation of

alkanethiols and disulfides monolayers on copper and silver is similar to that on gold. Unfortunately, there are few studies on the thermodynamics of alkanethiols adsorption on silver and copper. In fact, the studies of SAMs on silver and copper are substantially less extensive than those on gold. The reason might be rationalized by the difficulties in obtaining reproducible and high-quality SAMs on active metals (e.g. silver, copper, iron, etc.).

The detailed description of organosulfur SAMs will be presented in a later part.

2.2.2 Monolayers of organosilicon derivatives

SAMs of alkylchlorosilanes, alkylalkoxyxilanes, and alkylaminosilanes have been successfully assembled on various hydroxylated substrates, such as silicon oxide,^[25, 26] aluminum oxide,^[27] germanium oxide^[28] and gold.^[29] The driving force is the formation of the Si-O-Si bond connecting surface silanol groups on the substrate. The Si...Si distance is about 4.4 Å. A schematic drawing of organosilicon monolayer at a substrate interface is shown in Figure 2.2. SAMs of silanes are of significant importance due to many applications in industry. However, it is hard to get high-quality SAMs of alkylsilicon because the quality of the monolayer is very sensitive to formation conditions. Many factors, such as moisture and temperature, affect the formation, which might partly explain the differences, even contrary, in the results reported in the literature. Many efforts are devoted to achieving better reproducibility.

2.2.3 Monolayers of fatty acid

Fatty acid derivatives absorption on metal^[30-32] and metal oxide^[33, 34] surfaces is of interest because the interaction of fatty acid with substrate acts as a link between a Langmuir-Blodgett film and SAMs. It shows that the interaction between long-chain n-alkanoic acid and substrate is an acid-base reaction in which the driving force is the formation of a salt by reaction of metal cations with carboxylate anions. It was found that on a AgO surface, two oxygen atoms in the carboxylate group bind to the substrate surface displaying a tilt alkyl chain, while on the surfaces of CuO and Al₂O₃, the carboxylate asymmetrically binds to the surface resulting in an alkyl chain perpendicular to the surface. A schematic illustration of fatty acid monolayer structure is shown in Figure 2.3. Despite much works on this subject, there are still discrepancies in the structure, binding geometry and binding strength.

2.3 Sample Preparation

2.3.1 Substrate preparation

Many factors should be considered in choosing the substrate, including elements, crystalline state and quality. It is obvious that the surface treatment is crucial to the adsorption rate of the components and final quality of SAMs.

For inert elements, such as gold, the preparation process is relatively simple by evaporating gold onto silicon wafers, since it does not have a stable

surface oxide. In such a case, prior to the monolayer deposition, the substrate surface is treated with “piranha” solution (i.e. 3:7 H₂O₂/ concentrated H₂SO₄) at 90°C for 1h in order to remove the physically and chemically adsorbed contaminants, followed by rinse with Millipore water.^[35]

Although silver can form silver oxides in air, it would not exhibit catastrophic failures of monolayer adsorption on a limited-degree exposure to air. The degree of oxidation is also limited (i.e. one or two monolayers of silver oxides on the silver surface).^[36] Oxidized surfaces of silver are active to the chemisorption of alkanethiols, which probably involves reduction of Ag(I) to Ag(0) and direct conversion of surface Ag(I) oxides to Ag(I) thiolates. The surface cleaning procedure for silver is the same as that for gold.

However, for some reactive elements such as copper and iron, the formation of SAMs is much more difficult because the copper and iron surfaces readily form oxides that adsorb polar contaminants. Slightly oxidized surfaces of copper are subject to the chemisorption of alkanethiols; however, the formed monolayers differ in structure and properties from those formed on absolutely oxide-free surfaces. It is likely that the monolayer could form on a roughened copper/copper oxide interface and this monolayer might be heterogenous in structure. Therefore, to obtain reproducible and high-quality monolayers on both silver and copper, the metal surfaces should be clean and oxide-free. Oxygen must be completely excluded throughout the whole procedure.^[37] Occasionally, copper films manufactured even under oxygen-free conditions did not result in high-quality monolayers.^[37]

An electrochemical polishing method was also adopted to obtain an oxide-free copper surface. The sample treatment used by Vogt *et al.* included electrochemical polishing at 4V in 66% orthophosphoric acid for a few seconds, then Millipore water rinse, followed by polishing again at 1.8-2.4V for 10s.^[38, 39] This treatment is similar to that of Krufft *et al.*, who performed electrochemical polishing in 50% orthophosphoric acid at 2-2.4 V for 1 min to eliminate the oxide. Later, Vogt *et al.*^[39] modified their previous procedure by immersing the copper in 1 mM HCl for 5-10 mins after electrochemical polishing to obtain an oxide-free surface. However, it was suggested that chloride ions might adsorb on the copper surface, which would reduce the surface activity for adsorption.^[41]

Another surface treatment for a copper sample was galvanostatically reducing the specimen at a cathodic current density of 1 mA cm⁻² in 1M HClO₄ under nitrogen atmosphere protection for 10 min.^[42]

Recently, Feng *et al.* proposed a new method for copper treatment by etching the polished copper surface in 7M HNO₃ for 30 s and evaluating the effects of surface treatments on the quality of monolayers using impedance measurements.^[40] Their results demonstrated that HNO₃ etching was the most efficient way to form high quality films.

2.3.2 Assembly process

Up to now, the preparation of monolayers from solution has been most frequently employed. Monolayer deposition from a gas phase has succeeded in

some systems (e.g. SAMs of methanethiols were prepared from a gas phase).^[1]

Figure 2.4 shows the procedure of adsorption from solution.

It was found that high-quality monolayers were free of solvent molecules and the solvent had no effect on the structural differences of monolayers.^[37] The solubility of adsorbate, the reactivity of adsorbate and other considerations are the main criteria for solvent selection. Ethanol is the most frequently used solvent in solution preparation due to its low toxicity, low tendency to be incorporated into the monolayers and its high purity. For long-chain alkanethiols, hexadecane, THF, and isooctane were sometimes used for high solubility of thiols. However, the possibility of incorporating solvent into monolayers could not be negligible when the adsorbate and the solvent molecules are geometrically matched. In some specific cases, the solvent might even change the species of films. For instance, docosanethiol monolayer films could be adsorbed on copper from isooctane solution with high reproducibility. However, using the same procedure would often result in multilayers if adsorbed from ethanol solution.^[37] Therefore, the solvent should be selected with caution.

On the other hand, to avoid oxidization of unfunctional metal surfaces, adsorbate solution should be deoxygenated by bubbling with high-purity nitrogen or argon before transfer and throughout the immersion of the substrate.

The immersion time may vary from 15 minutes to several hours, depending on adsorbates and solvents. The concentrations of alkanethiols are in the range of micromolar per liter to millimolar per liter. Concentration and immersion time are parameters of significant importance. Longer immersion time and/or high

concentration of alkanethiols may result in the formation of “thicker” overlayers.^[20]

2.4 Characterization Techniques

There are many techniques employed to characterize SAMs. Those techniques are categorized according to their principles as follows.

2.4.1 Spectroscopy methods

Various spectroscopy methods are applied to SAMs to obtain information on the structure and their growth.

1. Infrared spectroscopy (IR)

Infrared spectroscopy is one type of vibrational spectroscopy where molecular vibrations are analyzed. Generally, IR is used to determine organic functional groups quantitatively. The vibration of CH₂ and CH₃ is always used to identify SAMs of alkanethiol. Nowadays, reflection Fourier transform infrared spectroscopy (FTIR) is widely used to obtain information on the structure, such as the chain conformation, orientation, coverage, and packing.^[22] A novel approach to analyze polarized IR spectra quantitatively has been described by Nuzzo *et al.*^[20, 21, 42] It did prove that different molecular orientations would account for the differences in spectra. The material constants were determined by an iterative procedure using a Kramers-Kronig transform, and the bulk spectra calculation involves Fresnel transmission coefficients. Its operation includes (1) the determination of the monolayer film’s isotropic optical functions; (2) estimation

of thickness of the film; (3) simulation of monolayer spectrum; (4) assignment of absorption feature to vibrational modes; (5) converting the dipole orientations to a molecular geometry. The parameters obtained by the above calculations will yield the average values of the tilt angle, α , and twist angle, β , around the molecular axis. This procedure will not be presented here in detail.

2. Photoelectron Spectroscopy

X-ray photoelectron spectroscopy (XPS) is a near-surface sensitive analytical technique involving core electrons. The binding energies of the core electrons can be determined by measuring the energy of the ejected electrons from an atom upon absorption of a photon. Shifts in the binding energy levels of different elements in the adsorbate and substrate are indicative of the changes in chemical character.^[44] This information can be used to identify and quantify the species in the surface. Therefore, XPS is capable of obtaining valuable chemical information to verify the composition of the adsorbate/substrate interface. Additionally, XPS may provide a convenient and rapid method for determining the thickness of SAMs by measuring the attenuation of photoelectrons from the substrate by the adsorbed layer.^[9] However, the probing depth of XPS is limited by the mean free path of photo-electrons, which is in the range of 1 to 5 nm.

3. Raman spectroscopy

Raman Spectroscopy is a universal analytical technique for identification of molecules in gases, liquids and solids by measuring the wavelength and intensity of the inelastically scattered light from molecules. The Raman scattered light occurs at wavelengths that are shifted from the incident light by the energies

of molecular vibrations. Nowadays, Raman spectroscopy, especially surface enhanced Raman Spectroscopy (SERS), is frequently applied to determine the composition of adsorbates. Kim *et al.* originally performed SERS characterization of SAMs.^[45] Raman spectroscopy results are also an index to identify the species adsorbed on a substrate surface.^[46]

4. Ellipsometry

Ellipsometry is an optical technique devoted to the analysis of surfaces. It is based on the measurement of the variation of the polarization state of light after reflection from a plane surface. The advantages of ellipsometry include its non-destructive character, its high sensitivity due to the measurement of the phase of the reflected light, its large measurement range (from fractions of monolayers to micrometers), and the possibilities of controlling complex processes in real time.

Ellipsometry is a valuable technique for measuring the film thickness of alkanethiols adsorbed on various metals.^[37]

5. Diffraction techniques

Diffraction techniques, such as low-energy atom diffraction (LEAD)^[47] and grazing-incidence X-ray diffraction (GIXD),^[48] also can provide information of two-dimensional structure of SAMs, provided the adsorbed layer with long-range order. Surface-sensitive electron diffraction techniques, such as low-energy electron diffraction spectroscopy (LEEDS) and reflectance high-energy electron diffraction spectroscopy (RHEEDS), are routinely used to monitor the structure of the adsorbed layer.^[44] However, these techniques have their own limitations, which should be noticed in the application.^[2]

2.4.2 Microscopy methods

Scanning tunneling microscopy (STM) and atomic force microscopy (AFM) are the most frequently used techniques, which may provide direct images of the local surface structure at the atomic level ($\sim 1 \text{ \AA}$) and characterize surface morphology at larger scales ($\sim 25 \text{ \AA}$) in environments ranging from ultra-high vacuum to aqueous solutions.^[49, 50] In addition, *in-situ* STM and/or AFM have been used for mechanism studies to provide information on the surfaces and the influence of SAMs on corrosion behavior.^[40]

STM has been used in the study of the structure of SAMs because it has a unique capacity to characterize local structure with atomic resolution.^[49, 50] A recent review has summarized the STM applications on structure determination, defects characterization, and assembly and decomposition mechanism verification.^[51] There have also been some studies correlating the STM images with electrochemical data.^[52] *In-situ* electrochemical scanning tunneling microscopy (ECSTM) has provided STM images during electrochemical processes.^[53]

Alves, *et al.* determined the structure of alkanethiolate on gold by AFM.^[54] The AFM images were attributed to the interactions between the AFM tip and the alkyl chain structure of this monolayer. It is also noteworthy that the imaging force was 50 nN, which is far beyond the upper-limit imaging force, i.e. in the order of 0.01 nN from model calculations.^[55] It was suggested that the strong cohesive inter-chain interactions and covalent bonding between sulfur head

group and gold surface enable the monolayers to withstand such large forces. Piner *et al.*^[56] developed a dip-pen nanolithography technique with a conventional AFM to study SAMs nucleation and growth kinetics.^[57]

2.4.3 Other methods

1. Contact angle measurement

Contact angle measurement is a technique to determine wettability, a macroscopic property of the surface studied. There is a hysteresis that exists between the advance and receding angle.

Hysteresis is greatest for a polar, heterogeneous and/or rough surface and for polar liquids; and least for a smooth, uniform surface and for nonpolar liquids. In the literature, water and hexadecane are often used as mediums.

Hysteresis phenomena are observed on most SAMs that are not wetted by the contacting liquid. In such cases, the wettability of SAMs is a useful parameter to evaluate the coverage of the monolayer. However, in fact, a surface hardly exhibits a unique, thermodynamic equilibrium contact angle. In practice, the maximum advancing angle is defined as the angle observed in the limit that the drop is advanced quasistatically over a motionless surface.^[58] An alternative method, developed by Whitesides *et al.*,^[59] is used to measure the kinetic energy of a fixed-sized drop of liquid advancing across the surface.

It has been demonstrated that both the advancing and receding angle are subject to the surface roughness, the relationship between observed angle, θ , and true angle, θ_{true} , on a smooth surface defined by the following equation:

$$\cos \theta = r \cos \theta_{\text{true}}$$

where r represents the surface roughness factor.

2. Kelvin probe

The Kelvin probe (or surface potential) method is a means to determine the work function difference between two surfaces and to estimate the adsorbate effects on the work function. It is a non-destructive technique based on the determination of capacitance between two separated surfaces, which form a capacitor with a charge due to the work function difference.^[44] The surface potential of monolayers was measured with respect to a reference (generally gold) by a Kelvin probe. It has been established that in thiolates of SAMs on a gold surface the adsorbed species is Au-SR, which is polar ($Au^{\delta+} - S^{\delta-}R$), and the bond has a net dipole moment with a permanent component perpendicular to the surface. Herein, it seems that the substrate surface is coated with a dipole sheet. This sheet would act as a potential barrier (electrostatic) when an electron tries to escape from the substrate surface. Hence, the work function ϕ will increase while the observed surface potential will decrease. The contact potential difference for the reference sample can be written as:

$$\phi_a - \phi_b = U_{\text{ref}} \quad (2-1)$$

where ϕ_a , and ϕ_b represent the work function of the vibrating electrode and reference electrode, respectively.

Considering that a SAMs-modified surface has a work function ϕ_b' , thus

$$\phi_a - \phi_b' = U_{\text{mon}} \quad (2-2)$$

therefore,

$$\phi_b - \phi_b' = U_{\text{mon}} - U_{\text{ref}} = \Delta U \quad (2-3)$$

If ΔU is positive, it means the work function ϕ_b' decreases and the surface dipole layer is oriented so that a sheet of negative charges lies close to the surface and a sheet of positive charges resides away towards the monolayer-ambient interface.^[35]

and ΔU obeys the following equation,^[60]

$$\Delta U = \mu_{\perp} / \epsilon \epsilon_0 V_m = \mu_{\perp} / \epsilon \epsilon_0 A \quad (2-4)$$

2.5 Structure

In this section, only the structure of full-coverage SAMs on a substrate surface is discussed. The balance of forces, which are interactions between thiol head groups and underlying substrate surface, van der Waals forces between the alkyl chains and interactions between endgroups, determine the structure of monolayers.^[51] Up to now, however, it is still impossible to determine the conformations and configurations of individual molecules in SAMs. All techniques to date only provide information on average microscopic structure. The structure of SAMs can be derived from both direct experimental data and computational simulations, including molecular dynamics methods (MD) and *Ab initio* calculations.^[5, 61]

FTIR and electron diffraction studies show that alkyl chains in SAMs of thiolate on Au(111) are usually tilted about 26-28° from the surface normal, and display 52-55° rotation around the molecular axis.^[62] A schematic diagram of an

all-trans chain orientation in an n-alkanethiol monolayer on gold surface is shown in Figure 2.5. The S...S distance in an assembly is 4.97 Å, which is larger than the distance of 4.6 Å, the distance between perpendicular alkyl chains in a close-packed layer. It also indicates that the alkyl chains are in the all-trans conformation. In general, the structure of monolayers on gold is described as a simple $(\sqrt{3} \times \sqrt{3})R30^\circ$ overlay, with an area per molecule of 21.6 Å².^[23, 54]

The nearest neighbor spacings in naked copper, silver, and Au (111) planes are 2.56 Å, 2.89 Å and 2.88 Å, respectively. It is reasonable to assume that the molecular orientations of the chains on silver are similar to those on gold and the average chain density on copper would be considerably higher than on gold or silver.

The chemisorption of sulfur atoms, SH and SCH₃ groups on Ag(111) can be described as that on Au(111), with an S...S distance of 4.41 Å, slightly smaller than the interchain repeat distance in crystalline paraffins of 4.65 Å. Also compared with those assembled on Au(111), monolayers on Ag(111) are more densely packed due to the shorter distance between chains.

Although quite different values of the tilt angle of alkanethiolates SAMs on silver are reported in literature, (e.g. 11-14° reported by Laibinis,^[37] 7° by Ulman,^[63] while even 0° suggested by Nemetz and Fenter^[63]), one conclusion was reached unanimously: that the alkyl chains of alkanethiolates are more perpendicular to clean silver surface than those on a gold surface and the

monolayer is more close-packed on silver than on gold. Unlike on gold, the structure of short chain linear monolayers on silver can be described as $(\sqrt{7} \times \sqrt{7})R10.9^\circ$. However, there is still some debate on the structure of long-chain monolayers on silver. Furthermore, if the chain contains a bulky group (e.g. *tert* butyl), the structure is much more complex and depends on the interchain interactions.

The differences in the structure of monolayers formed on gold and silver are striking and interesting, which has been assigned to the differences in the reactivity of the surfaces of the metal, especially their susceptibilities to oxidation upon exposure to air. When exposed to air, the surface of silver slightly oxidized, under ambient conditions one or two monolayers of silver oxide are formed on the silver surfaces.^[64] For their [111] lattices, gold and silver differ in the surface energy morphology, (e.g., in peak-to-valley energy difference is $6.0 \text{ kcal mol}^{-1}$ for gold but is only $3.3 \text{ kcal mol}^{-1}$ for silver).^[5] The valleys are the most favored binding sites (hollow sites), the peaks are the least favored sites (on-top sites). Therefore, even though surfaces of Au(111) and Ag(111) are atomically flat, site selection of adsorption exists due to the energetical heterogeneity.

Thiolates on Au(111) only occupy the most energy-favored sites (i.e. every sixth hollow site), forming a $(\sqrt{3} \times \sqrt{3})R30^\circ$ overlayer.^[23, 65, 66] However, on Ag(111), adsorption at an on-top site could compete with that at a hollow site due to the small peak-to-valley energy difference. These different adsorption patterns explain the structure differences: for thiolates on Ag(111), the most effective

absorption structure has a spacing about 4.4 Å and the molecular axis normal to the surface,^[67] however, on Au(111), the most effective spacing is near 5.0 Å with a molecular axis tilted about 30°. If SAMs on gold had the same structure as those on silver, they would not be stable due to the chemisorption potentials and charge-charge repulsion.

The difference between alkanethiolate SAMs on Au(111) and Ag(111) might also result from the interplay of chemisorption and chain-chain interactions. For example, the S...S distance for methanethiolate on Ag(111) is 4.41 Å, which fits well with the distance of 4.41 Å obtained from the most effective spacing; however, the distance is about 4.6 Å for a long alkyl chains monolayer on Ag(111). The chain-chain van der Waals interaction is believed to cause the differences.

For SAMs on copper, there is little structural information available in the literature. The reason might be the poor reproducibility of the test results. The structure of SAMs formed on copper is extremely sensitive to the history of the sample and experimental techniques in sample preparations. High quality films on copper are composed of closest packed chains with significantly shorter interchain spacings than that on gold; on the contrary, poorer quality films contain a great amount of disorder. This is because the surfaces of copper oxidize rapidly upon exposure to air.

2.6 Kinetic of adsorption

Kinetics of formation of SAMs is relatively complex because the rate of adsorption is influenced by many factors, some of which are easily controlled, such as temperature, solvent, and adsorbate concentration, and others are inherent to the system, such as reactivity of surface atoms, chain-chain interactions and reversibility of reaction at surfaces.

Based on two different kinetics involved in the whole adsorption process, linear chain monolayer growth kinetics is insightfully proposed by Bain *et al.*^[59] The initial step is the formation of an imperfect monolayer via very fast adsorption of SAMs molecules on the substrate surface. This step lasts a few minutes. At the end of the initial step the contact angles are close to the final values and the thickness is about 80-90% of its maximum value. The second step is a slow process of additional adsorption and consolidation, which takes a long time from several hours to even several days. At the end of the second step all parameters reach their own final values. In this step, solvent included in the monolayer is gradually expelled and defects are repaired by lateral diffusion.

For a long linear alkyl chain monolayer, this mechanism is followed quite well. This two-step mechanism was confirmed by various studies and has been generally accepted by other researchers. In fact, some other factors, such as steric effects, surface roughness and contamination, probably have considerable impact on the total kinetics. In some cases, included solvent still remains in the monolayers. (As the authors mentioned, experimental conditions must have a

significant role in each system employed.) Recent investigations shed new light on this topic.

Evans *et al.* investigated the chain steric effects on the total kinetics.^[34] It is found that if the chain contains a bulky group (e.g. aromatic groups), the chemisorption kinetics is greatly impeded by the chain disorder.^[68]

Recently, Hong *et al.* proposed a similar monolayer growth mechanism from their nanolithography studies.^[56] Based on their results, the formation of SAMs is initialized by a relatively slow nucleation process, followed by a fast island monolayer growth process, and finally accomplished by a slow saturation process. It was also pointed out that adsorption and desorption processes might play an important role in the formation of the final equilibrium structure of the monolayers. Admittedly, the two-step mechanism with other modifications should be regarded as a general case; for each new system, the kinetics should be reestablished with specified experiment conditions.

2.7 Stability of SAMs

The implementation of SAMs into industrial applications is largely depended on the stability of these films under ambient and extreme conditions.^[69] The deterioration of alkanethiol SAMs under thermal stress or long time exposure to air has been widely reported.

2.7.1 Thermal stability of SAMs

The thermal durability of alkanethiolate SAMs under ambient atmosphere has been addressed in the literature. It has been found that SAMs could be stable within moderate temperature range. The deterioration of SAMs by thermal stress will result in the loss of order in the monolayers.

Nuzzo *et al.* first demonstrated loss of sulfur from SAMs of hexadecanethiolate on gold over the temperature range of 150-200 °C.^[6] IR results indicated that the thermal-induced structure changes were reversible below 125 °C; however, these changes became irreversible when heating up to 150 °C. Partial desorption of the adsorbate or structure restructuring might occur at 150 °C. When the temperature increases to near 200 °C, no adsorbate is left on the substrate. Differential scanning calorimetry (DSC) studies have also revealed that the thermal behavior of surface-adsorption molecules significantly differs from that of the bulk materials. Furthermore, the adsorption bond energy was estimated from thermal desorption results.^[20, 70]

In their later work, Nuzzo *et al.* performed temperature-programmed desorption of methanethiolate SAMs on gold. It was reported that the desorption was a molecular process, i.e., there was no ionization involved in the desorption. The substrate surface was clean after desorption.^[43, 47]

In a detailed mass spectroscopic study, Jaffey and Madix illustrated the desorption mechanism of a *tert*-butyl thiolate monolayer on gold. The *tert*-butyl thiolate is stable up to about 130°C and a maximum desorption is at about 200°C. In their opinion, the main decomposition might occur via a disproportion reaction between two adsorbed thiolate molecules in SAMs, resulting in a thiol molecule

with one alkene, and adsorbed sulfur on gold. The formation of H₂S might be the result of a direct reaction of the thiol and adsorbed sulfur.^[71]

A STM/XPS study of dodecanethiol SAMs on gold showed surface phase changes accompanying the loss of thiolates.^[72] It showed that no surface change occurred below 85 °C. Their STM/XPS study also revealed that desorption competed with thiolate oxidation and alkylsulfonates remained in the monolayer for temperature less than 100 °C. At 100 °C, the top layer of the gold mobilized and the depressions fused with terrace edges forming larger domains, resulting in a lack of thiolate molecules.

Recently, Schlenoff *et al.* reported that for a monolayer of 1-octadecanethiol self-assembled on gold, a complete loss of sulfur occurred at 210 °C.^[19] However, the desorption process occurred in a wide temperature range with partial loss at 100 °C. Desorption increases and coverage decreases with increasing temperature.

The thermal stability of SAMs is largely related to the monolayer species, quality of SAMs, and the environment. Herein, the thermal sensitivity of SAMs-coated metals should have a significant impact on their applications.

2.7.2 Stability of SAMs in air

It has been well established that alkanethiol-SAMs are extraordinarily inert under ambient conditions.^[1, 8, 73] However, organothiol monolayers on gold exposed to air for prolonged periods have been shown to oxidize to sulfinates and sulfonates, suggesting their stability is limited.^[18, 74-76] Once oxidized, aromatic

sulfonates have been claimed to subsequently desorb upon aqueous washing, indicating weaker surface affinity than the original SAMs. In addition, it has been established that oxidized SAMs rapidly exchange with thiols when placed in fresh thiol solution.^[74, 76-78]

Using laser-desorption Fourier transform mass spectrometry (LD-FTMS), Li *et al.*^[18] first reported the formation of sulfonate resulting from air exposure of alkanethiol-SAMs [$\text{CH}_3(\text{CH}_2)_n\text{SH}$, $n = 3, 5, 7, 8, 11, 15$, and 17] adsorbed on gold. Unfortunately, neither the extent of oxidation nor the rate of the oxidation process was determined in their work. Their result was confirmed by Tarlov and Newman by using static secondary ion mass spectrometry (SSIMS).^[73] It was found that the sulfonate species formed in the oxidation process were replaced by thiols when reimmersed into solution. In fact, no sulfonate species was detected with SSIMS from any SAMs stored in air-saturated thiol/ethanol adsorbated solution for periods up to 2 months, indicating that any sulfonates formed are continuously displaced by thiol molecules. However, contrary to the reports by Li *et al.* and Tarlov and Newman, Scott *et al.*^[75] suggested the possibility of SAMs being extensively oxidized in air in the study of the exchanging of $\text{CH}_3(\text{CH}_2)_{11}\text{SH}$ SAMs on gold with $\text{CH}_3(\text{CH}_2)_9\text{SH}$ using LD-FTMS.

In an IR study of the aging of alkanethiol SAMs^[79], a change in the relative intensities of the $\nu(\text{C-H})$ bands was observed, suggesting a tilting of alkanethiol molecules away from the surface normal. Based on their observation, Horn *et al.* proposed that the SAMs restructuring is due to alkanethiol oxidation at the sulfur head group.

UV-assisted oxidation of alkanethiol SAMs on gold has been widely investigated.^[78, 80-85] Photooxidation of SAMs has received considerable attention due to its potential for selective patterning of gold surfaces.^[78, 80] Rieley *et al.*^[81] used near-edge extended X-ray absorption fine structure and ultraviolet photoemission spectroscopy to study the photooxidation of $\text{CH}_3(\text{CH}_2)_7\text{SH}$ SAMs on Au (111). They theorized that incident UV radiation absorbed by the gold surface produces O^{2-} , which can subsequently oxidize adsorbed thiolate species to the sulfonates. Extensive sulfonate formation was observed in the region of the surface exposed to UV light.

Hutt and Leggett studied the effects of UV irradiation of methyl-terminated alkanethiol SAMs [$\text{CH}_3(\text{CH}_2)_n\text{SH}$, $n = 2, 5, 7, 9, 11, 15,$ and 17] on gold using XPS.^[84] They also observed significant thiolate oxidation to sulfonate species by “active” O species as a result of UV exposure. The rate of photooxidation was found to vary significantly with alkyl chain length; short-chain-length SAMs oxidize much faster than long-chain SAMs.

Lewis *et al.*^[82] studied the photooxidation process of alkanethiol SAMs [$\text{CH}_3(\text{CH}_2)_n\text{SH}$, $n = 5, 9,$ and 17] on electrochemically roughened silver using surface enhanced Raman scattering (SERS) and concluded that UV irradiation in air photochemically induces C-S bond scission. The alkyl chain fragments subsequently desorb so that the surface-bound sulfur is exposed to the air and is oxidized.

Recently, Schoenfisch *et al.*^[85] studied the effect of ambient laboratory air without UV irradiation or light exposure on the structure of SAMs

[CH₃(CH₂)_nSH, n = 2, 11, and 17] formed on silver and gold surfaces by using XPS and Raman spectroscopy. Their results clearly demonstrate oxidation of alkanethiol SAMs on silver and gold upon air exposure in the absence of light. However, the extent of oxidation is small after one week of dark air exposure and these SAMs still generally retain their integrity with respect to electron transfer blocking properties. It was also inferred that the oxidation rate varies strongly with alkyl chain length. Long-chain-length SAMs oxidized much more slowly due to the inability of the active oxidant species to penetrate the closely packed alkyl chain structure. Short-chain SAMs oxidize faster as a result of shorter distances between the outside of the SAM and sulfur headgroup and the greater number of defects. Poorly formed films containing large number of defects are less stable.

Despite the interest in using SAMs for a variety of applications, few studies have thoroughly investigated alkanethiol oxidation in an ambient laboratory environment by spectroscopic techniques. The air stability of SAMs may be of considerable importance to the photopatterning community because of the need to selectively control oxidation.^[86]

Many factors affect alkanethiol oxidation, including chain length, initial film quality, nature of the metal substrate, and atmospheric ozone (O₃) levels. Conflicting reports on the stability of SAMs in air are probably due to a combination of the above factors; however, the concentration of O₃ in laboratory air might be the determining factor.

2.7.3 Stability of SAMs in corrosive solution

As far as our knowledge goes, there have been few investigations on the electrochemical stability of SAMs in aqueous solutions.

In their electrochemical stability study of organosulfur-forming SAMs on gold, Beulen *et al.* found the SAMs could retain their integrity within a limited potential range in 0.1 M K₂SO₄.^[87] In their work, charge-transfer resistance was chosen as the parameter to evaluate the electrochemical stability of SAMs, which remains constant within a certain potential range and exhibits a rapid decay outside that range. The potential range varies with the species and quality of SAMs. Unfortunately, the authors provided little information on the origin of the destruction of the monolayer beyond the potential range.

Zamborini and Crooks^[53] provided an elegant explanation for the corrosion passivation of gold by n-alkanethiol in aqueous halide solution. For gold modified by hydrophobic SAM, pitting corrosion occurred on the substrate surface. Since the surface of SAM was hydrophobic, halide ions could access gold and attack the surface only at the defects within the monolayer. The initial pits in gold expanded preferentially in the gold surface plane. Gold dissolved within the pits accompanying desorption of some thiol molecules. At a higher potential, it dissolved downward in a stepwise manner and resulted in deeper and wider pitting.^[88] Some thiols around the pits desorbed from the monolayer while others reoriented more parallel to the surface plane. This means that the thiols were disordered in and around the vicinity of the pits; however, the monolayer remained ordered at the region between pits. Figure 2.6 shows the illustration of

the mechanism. Their corrosion mechanism is partly in contrast to that of Scherer's,^[40] which suggested a similar pitting mechanism but no thiols left in the pits. The initial corrosion of a gold surface covered by hydrophilic SAM is similar to that modified by hydrophobic SAM; i.e. pits started at defects in the monolayer and expanded along the surface plane. Since hydrophilic SAMs are more mobile on the surface in aqueous solutions, deep pitting was inhibited by the reorientation of thiols that were on the original terrace. Finally, all thiols were parallel to the surface in a tail-to-tail conformation, which is energy favored due to the formation of hydrogen bonding between the end groups. Therefore, corrosion occurred in a smooth layer-by-layer pattern and no deep pits were observed. This mechanism is illustrated in Figure 2.7.

2.8 Applications and future work

To date, many studies on SAMs have focused on ways for chemical modification of SAMs to build new structures with novel properties.^[19]

2.8.1 Intermolecular interactions and surface engineering in

SAMs

SAMs offer a vehicle for understanding of interfacial phenomena, self-organization, and structure-property relationships. SAMs also provide the flexibility for materials and individual molecule design and engineering.

The stability of the monolayer can be improved simply by introducing specific interchain interactions into the SAMs. Additional dipole-dipole and/or hydrogen bonding interactions will result in the enhancement of ordering and packing in the monolayer. Experimental results and molecular dynamics simulations have proved that sulfone (-SO₂-) groups in the alkyl chain could increase the dipole-dipole interactions between chains. It is evident that the strong electrostatic interactions between SO₂ groups would promote the formation of a dipole plane within the assembly, which affects the packing and ordering of the monolayers.^[89] Further studies have revealed that the monolayer stability against desorption and exchange rate is significantly improved by introduction of amide (-NHCO-) groups into the alkyl chain resulting in intermolecular H-bonding. Compared with original SAMs, the exchange rate is 100 to 1000 times slower for the SAMs modified by an amide group. At 10⁻⁹ torr, no desorption occurred from CF₃CH₂NHCOCH₂SH SAMs on gold for at least 48h. However, at 10⁻⁹ Torr, desorption from CF₃(CH₂)₃SH SAMs on gold had a half-life time of about 2h.^[90]

Alkanethiol SAMs with functional endgroups are important for surface engineering and for further chemical reactions. A monolayer of carboxylate-terminated alkanethiols can react with alkanolic acids and amines to form a bilayer structure. Furthermore, the carboxylate group can be transformed to the corresponding acid chlorides, which can further yield amides and esters. By repeated similar procedures, polymeric SAMs and multilayers of thiolester were obtained by Kim *et al.* SAMs with terminal hydroxy group have even more applications in surface modifications. For instant, the OH group can be cross-

linked with alkyltrichlorosilane and water to form two-dimensional polymer monolayers, which are more resistant to diffusion of O₂ and penetration of corrosive ions.^[42, 91, 92] SAMs with OH terminal groups also can react with OTS,^[93] with POCl₃,^[94-96] with anhydrides,^[97] with alkylisothiocyanate,^[98] etc. Prucker and R  he modified the endgroup of SAMs on gold to an initiator.^[99] Further polymerization reactions were initiated. These new types of SAMs not only considerably enlarge the region of SAMs but also provide a great opportunity for studies of molecular recognition, electron transfer, interface phenomena, etc.

2.8.2 Corrosion protection by SAMs

Additionally, SAMs offer the possibility of protecting metals from corrosion in corrosive media. The advantages of SAMs over common organic coatings are: (i) the film forms through a simple chemisorption process and strongly adheres to the metal surface and, (ii) their thickness can be controlled at the nanometer level by selecting adsorbates and, (iii) they do not significantly alter the appearance or most other characteristics of the substrate except changing hydrophilicity of the metal surfaces. Theoretically, the hydrophobic alkanethiol SAMs are ionic insulators, being able to isolate the metal surface from the corrosive solutions. However, there have been few corrosion studies of copper surfaces modified with alkanethiols up to now, as far as our knowledge goes.

2.9 Summary

It is concluded from the studies reported that self-assembly of alkanethiol monolayers on copper and iron substrates is relatively difficult because copper and iron oxidize easily. Copper is a metal widely used in chemical and electronics industries due to its high thermal and electrical conductivities and low cost. Obviously, it is more valuable to prepare alkanethiol SAMs on copper substrates than on gold substrates from the viewpoint of practical application. Additionally, the techniques for self-assembling the monolayers on copper, especially the surface pretreatment process, requires improvement. In addition, more characterizations concerning properties of alkanethiol SAMs on copper should be carried out. Therefore, we choose to prepare and study SAMs of three n-alkanethiols with different chain lengths on a copper substrate in this work.

2.10 Reference

- [1] A. Ulman, *Chem. Rev.* **1996**, *96*, 1533.
- [2] F. Schreiber, *Prog. Surf. Sci.* **2000**, *65*, 151.
- [3] A. Ulman, *An Introduction to Ultrathin Organic Films: From Langmuir-Blodgett to Self-Assembly*, Academic Press, New York, **1991**.
- [4] L. H. Dubois, R. G. Nuzzo, *Annu. Rev. Phys. Chem.* **1992**, *43*, 437.
- [5] H. Sellers, A. Ulman, Y. Shnidman, J. E. Eilers, *J. Am. Chem. Soc.* **1993**, *115*, 9389.
- [6] R. G. Nuzzo, D. L. Allara, *J. Am. Chem. Soc.* **1983**, *105*, 4481.
- [7] M. M. Walczak, C. Chung, S. M. Stole, C. A. Widrig, M. D. Porter, *J. Am. Chem. Soc.* **1991**, *113*, 2370.
- [8] P. E. Laibinis, G. M. Whitesides, *J. Am. Chem. Soc.* **1992**, *114*, 9022.
- [9] P. E. Laibinis, R. G. White, *J. Am. Chem. Soc.* **1992**, *114*, 1990.
- [10] N. Muskal, I. Turyan, A. Shurky, D. Mandler, *J. Am. Chem. Soc.* **1995**, *117*, 1147.
- [11] M. Stratmann, *Adv. Mater.* **1990**, *29*, 191.

- [12] Q. Liu, Z. Xu, *Langmuir* **1995**, *11*, 4617.
- [13] C. D. Bain, *Adv. Mater.* **1992**, *4*, 591.
- [14] C. W. Sheen, J. X. Shi, J. Martensson, A. N. Parikh, D. L. Allara, *J. Am. Chem. Soc.* **1992**, *114*, 1514.
- [15] Y. Gu, B. Lin, V. S. Smentkowski, D. H. Waldeck, *Langmuir* **1995**, *11*, 1849.
- [16] J. Zak, H. Yuan, M. Ho, K. Woo, M. D. Porter, *Langmuir* **1993**, *9*, 2722.
- [17] X. Shi, B. Caldwell, K. Chen, C. A. Mirkin, *J. Am. Chem. Soc.* **1994**, *116*, 11598.
- [18] Y. Li, J. Huang, J. R. T. McIver, J. C. Hemminger, *J. Am. Chem. Soc.* **1992**, *114*, 2428.
- [19] J. B. Schlenoff, M. Li, H. Ly, *J. Am. Chem. Soc.* **1995**, *117*, 12528.
- [20] R. G. Nuzzo, F. A. Fusco, D. L. Allara, *J. Am. Chem. Soc.* **1987**, *109*, 2358.
- [21] R. G. Nuzzo, L. H. Dubois, D. L. Allara, *J. Am. Chem. Soc.* **1990**, *112*, 558.
- [22] M. D. Porter, T. B. Bright, D. L. Allara, C. E. D. Chidsey, *J. Am. Chem. Soc.* **1987**, *109*, 3559.
- [23] L. Strong, G. M. Whitesides, *Langmuir* **1988**, *4*, 546.
- [24] H. A. Biebuyck, C. D. Bain, G. M. Whitesides, *Langmuir* **1994**, *10*, 1825.
- [25] J. Sagiv, *J. Am. Chem. Soc.* **1980**, *102*, 92.
- [26] J. D. Le Grange, J. L. Markham, C. R. Kurjian, *Langmuir* **1993**, *9*, 1749.
- [27] N. Tillman, A. Ulman, J. S. Schildkraut, T. L. Penner, *J. Am. Chem. Soc.* **1988**, *110*, 6136.
- [28] J. Gun, J. Sagiv, *J. Colloid Interface Sci.* **1986**, *112*, 457.
- [29] H. O. Finklea, L. R. Robinson, A. Blackburn, B. Richter, D. L. Allara, T. Bright, *Langmuir* **1986**, *2*, 239.
- [30] D. L. Allara, R. G. Nuzzo, *Langmuir* **1985**, *1*, 45.
- [31] Y. T. Tao, G. D. Hietpas, D. L. Allara, *J. Am. Chem. Soc.* **1996**, *118*, 6724.
- [32] N. E. Schlotter, M. D. Porter, T. B. Bright, D. L. Allara, *Chem. Phys. Lett.* **1986**, *132*, 93.
- [33] Y. T. Tao, *J. Am. Chem. Soc.* **1993**, *115*, 4350.
- [34] S. D. Evans, E. Urankar, A. Ulman, N. Ferris, *J. Am. Chem. Soc.* **1991**, *113*, 4121.
- [35] G. Rovida, F. Pratesi, *Surf. Sci.* **1975**, *52*, 542.
- [36] P. E. Laibinis, G. M. Whitesides, D. L. Allara, Y.-T. Tao, A. N. Parikh, R. G. Nuzzo, *J. Am. Chem. Soc.* **1991**, *113*, 7152.
- [37] M. R. Vogt, F. A. Mo"ller, C. M. Schilz, O. M. Magnussen, R. J. Behm, *Surf. Sci.* **1996**, *367*, L33.
- [38] M. R. Vogt, A. Lachenwitzer, O. M. Magnussen, R. J. Behm, *Surf. Sci.* **1998**, *399*, 49.
- [39] J. Scherer, M. R. Vogt, O. M. Magnussen, R. J. Behm, *Langmuir* **1997**, *13*, 7045.

- [40] Y. Feng, W.-K. Teo, K.-S. Siow, Z. Gao, K.-L. Tan, A.-K. Hsieh, *J. Electrochem. Soc.* **1997**, *144*, 55.
- [41] M. Itoh, Nishihara, K. H. Aramaki, *J. Electrochem. Soc.* **1995**, *142*, 1839.
- [42] R. G. Nuzzo, B. R. Zegarski, L. H. Dubois, *J. Am. Chem. Soc.* **1990**, *112*, 733.
- [43] F. Seker, K. Meeker, T. F. Kuech, A. B. Ellis, *Chem. Rev.* **2000**, *100*, 2505.
- [44] J.-H. Kim, T. M. Cotton, R. A. Uphaus, *Thin Solid films* **1988**, *160*, 389.
- [45] M. A. Bryant, J. E. Pemberton, *J. Am. Chem. Soc.* **1991**, *113*, 3629.
- [46] N. Camillone, C. E. D. Chidsey, G.-Y. Liu, G. Scoles, *J. Chem. Phys.* **1993**, *98*, 3503.
- [47] P. Fenter, P. Eisenberger, K. S. Liang, *Phys. Rev. Lett.* **1993**, *70*, 2447.
- [48] G. E. Poirier, M. J. Tarlov, *Langmuir* **1994**, *10*, 2853.
- [49] E. Delamarche, B. Michel, C. Gerber, D. Anselmetti, H.-J. Guntherodt, H. Wolf, H. Ringsdorf, *Langmuir* **1994**, *10*, 2869.
- [50] G. E. Poirier, *Chem. Rev.* **1997**, *97*, 1117.
- [51] D. J. Trevor, C. E. D. Chidsey, D. N. Loiacono, *Phys. Rev. Lett.* **1989**, *62*, 929.
- [52] F. P. Zamborini, R. M. Crooks, *Langmuir* **1998**, *14*, 3279.
- [53] C. A. Alves, E. L. Smith, M. D. Porter, *J. Am. Chem. Soc.* **1992**, *114*, 1222.
- [54] B. N. Persson, *Chem. Phys. Lett.* **1987**, *141*, 366.
- [55] R. D. Piner, J. Zhu, F. Xu, S. Hong, C. A. Mirkin, *Science* **1999**, *283*, 661.
- [56] S. Hong, J. Zhu, C. A. Mirkin, *Langmuir* **1999**, *15*, 7897.
- [57] R. H. Dettre, R. E. Johnson, *J. Phys. Chem.* **1965**, *69*, 1507.
- [58] O. Oliveira, Jr., D. M. Taylor, T. J. Lewis, S. Salvagno, J. M. Stirling, *J. Chem. Soc., Faraday Trans.* **1989**, *85*, 1009.
- [59] C. D. Bain, E. B. Throughton, Y. T. Tao, J. Evall, G. M. Whitesides
R. G. Nuzzo *J. Am. Chem. Soc.* **1989**, *111*, 321
- [60] J. Hautman, M. L. Klein, *J. Chem. Phys.* **1989**, *91*, 4994.
- [61] R. G. Nuzzo, E. M. Korenic, L. H. Dubois, *J. Chem. Phys.* **1990**, *93*, 767.
- [62] A. Nemetz, T. Fischer, A. Ulman, W. Knoll, *J. Chem. Phys.* **1993**, *98*, 5912.
- [63] H. A. Englehardt, D. Menzel, *Surf. Sci.* **1976**, *57*, 591.
- [64] C. E. D. Chidsey, D. N. Loiacono, *Langmuir* **1990**, *6*, 709.
- [65] L. H. Dubois, B. R. Zegarski, R. G. Nuzzo, *J. Chem. Phys.* **1993**, *98*, 678.
- [66] A. Ulman, J. E. Eilers, N. Tillman, *Langmuir* **1989**, *5*, 1147.
- [67] D. A. Offord, C. M. John, M. R. Linfood, J. H. Griffin, *Langmuir* **1994**, *10*, 883.
- [68] H. Fukushima, S. Seki, T. Nishikawa, H. Takiguchi, K. Tamada, K. Abe, J. Colorado, R., M. Graupe, O. E. Shmakova, T. R. Lee, *J. Phys. Chem. B* **2000**, *104*, 7417.
- [69] J. J. Hickman, D. Ofer, C. Zou, M. S. Wrighton, P. E. Laibinis, G. M. Whitesides, *J. Am. Chem. Soc.* **1991**, *113*, 1128.
- [70] D. M. Jaffery, R. J. Madix, *J. Am. Chem. Soc.* **1994**, *116*, 3012.

- [71] E. Delamarche, B. Michel, H. Kang, C. Gerber, *Langmuir* **1994**, *10*, 4103.
- [72] A. K. Kumar, H. A. Biebuyck, G. M. Whitesides, *Langmuir* **1994**, *10*, 1498.
- [73] M. J. Tarlov, J. G. Newman, *Langmuir* **1992**, *8*, 1398.
- [74] A. B. Hornm, D. A. Russell, L. J. Shorthouse, T. R. E. Simpson, *J. Chem. Soc., Faraday Trans.* **1996**, *92*, 4759.
- [75] J. R. Scott, L. S. Baker, W. R. Everett, C. L. Wilkins, I. Fritsch, *Anal. Chem* **1997**, *69*.
- [76] R. L. Garrell, J. E. Chadwick, D. L. Severance, N. A. McDonald, D. C. Myles, *J. Am. Chem. Soc.* **1995**, *117*.
- [77] J. Huang, J. C. Hemminger, *J. Am. Chem. Soc.* **1993**, *115*, 3342.
- [78] A. B. Horn, D. A. Russell, L. J. Shorthouse, T. R. E. Simpson, *J. Chem. Soc., Faraday Trans.* **1996**, *92*, 4759.
- [79] M. J. Tarlov, J. Burgess, D. R. F., G. Gillen, *J. Am. Chem. Soc.* **1993**, *115*, 5305.
- [80] J. Huang, D. A. Dahlgren, J. C. Hemminger, *Langmuir* **1994**, *10*, 626.
- [81] H. Rieley, N. J. Price, R. G. White, R. I. R. Blyth, A. B. Robinson, *Surf. Sci.* **1995**, *331-333*, 189.
- [82] M. Lewis, M. J. Tarlov, K. Carron, *J. Am. Chem. Soc.* **1995**, *117*, 9574.
- [83] J. M. Behm, K. R. Lykke, M. J. Pellin, J. C. Hemminger, *Langmuir* **1996**, *12*, 2121.
- [84] D. A. Hutt, G. L. Leggett, *J. Phys. Chem.* **1996**, *100*, 6657.
- [85] M. H. Schoenfish, J. E. Pemberton, *J. Am. Chem. Soc.* **1998**, *120*, 4502.
- [86] M. W. Beulen, M. I. Kastenber, F. C. J. M. v. Veggel, D. N. Reinhoudt, *Langmuir* **1998**, *14*, 7463.
- [87] O. M. Magnussen, B. M. Ocko, J. X. Wang, R. R. Adzic, *J. Phys. Chem.* **1996**, *100*, 5500.
- [88] S. D. Evans, K. Goppert-Berarducci, E. Urankar, L. J. Gerenser, A. Ulman, *Langmuir* **1991**, *7*, 2700.
- [89] S.-W. Tam-Chang, H. A. Biebuyck, G. M. Whitesides, N. Jeon, R. G. Nuzzo, *Langmuir* **1995**, *11*, 4371.
- [90] M. Itoh, H. Nishihara, K. Aramaki, *J. Electrochem. Soc.* **1994**, *141*, 2018.
- [91] R. Haneda, H. Nishihara, K. Aramaki, *J. Electrochem. Soc.* **1997**, *144*, 1215.
- [92] A. Ulman, N. Tillman, *Langmuir* **1989**, *5*, 1418.
- [93] M. L. Schilling, H. E. Katz, S. M. Stein, S. F. Shane, W. L. Wilson, S. Buratto, S. B. Ungahse, G. N. Taylor, T. M. Putvinski, C. E. D. Chidsey, *Langmuir* **1993**, *9*, 2156.
- [94] L. Bertilsson, B. Liedberg, *Langmuir* **1993**, *9*, 141.
- [95] S. F. Bent, M. L. Schilling, W. L. Wilson, H. E. Katz, A. L. Harris, *Chem. Mater.* **1994**, *6*, 122.
- [96] S. D. Evans, R. Sharma, A. Ulman, *Langmuir* **1991**, *7*, 156.
- [97] S. Löfs, B. Johnsson, *J. Chem. Soc., Chem. Commun.* **1990**, 1526.
- [98] O. Prucker, J. Rühle, *Langmuir* **1998**, *14*, 6893.

Figures in Chapter 2.

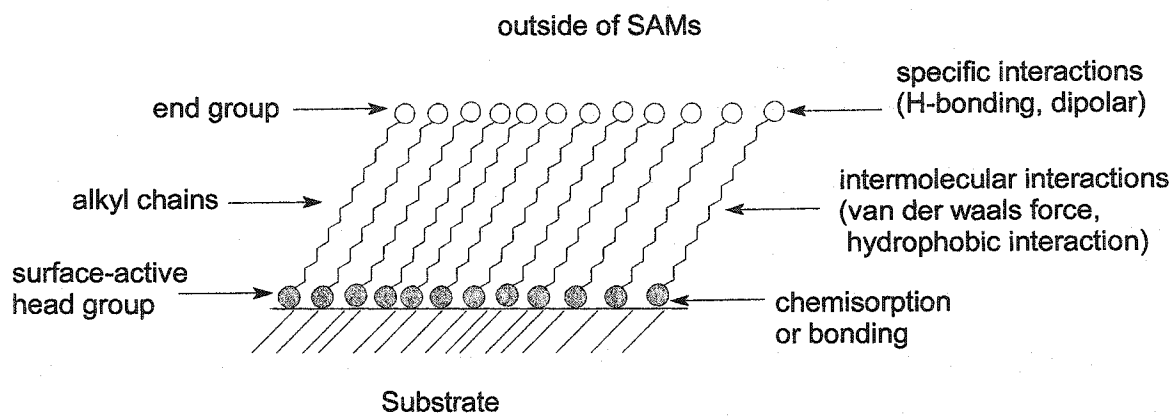


Figure 2.1. A schematic graph of Self-assembled monolayers [1]

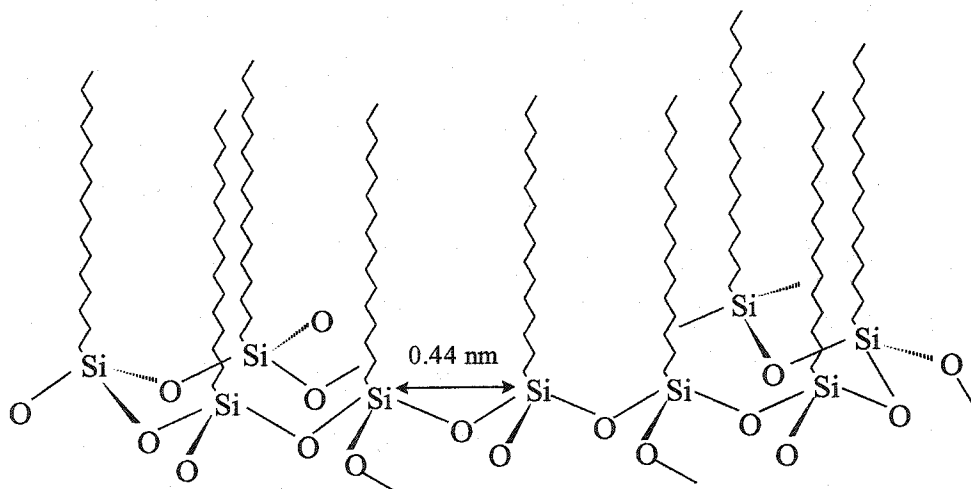


Figure 2.2. A schematic graph of organosilicon monolayer at substrate surface [1]

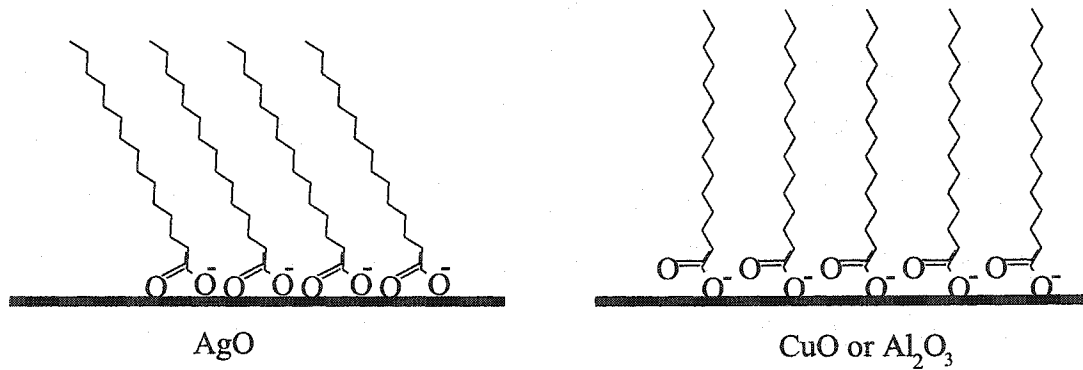


Figure 2.3. A schematic illustration of fatty acid monolayer structure

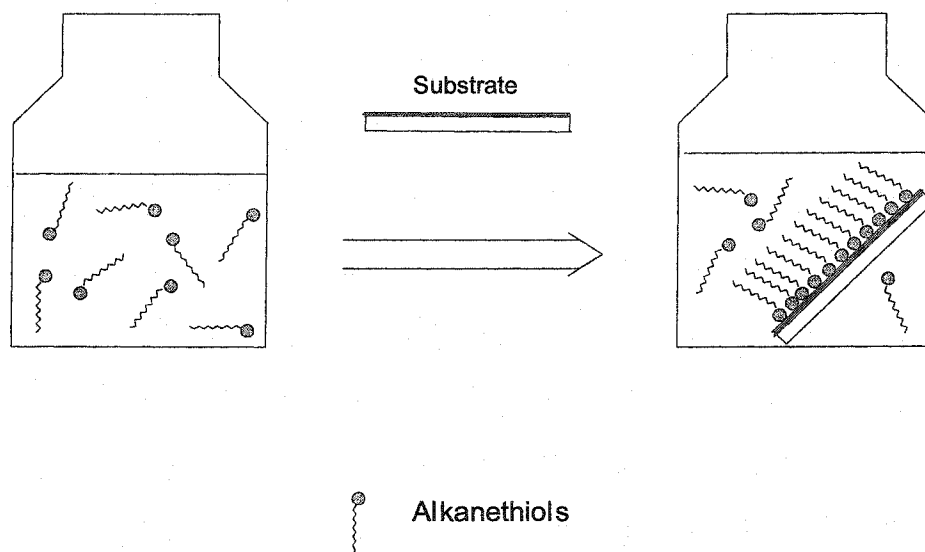
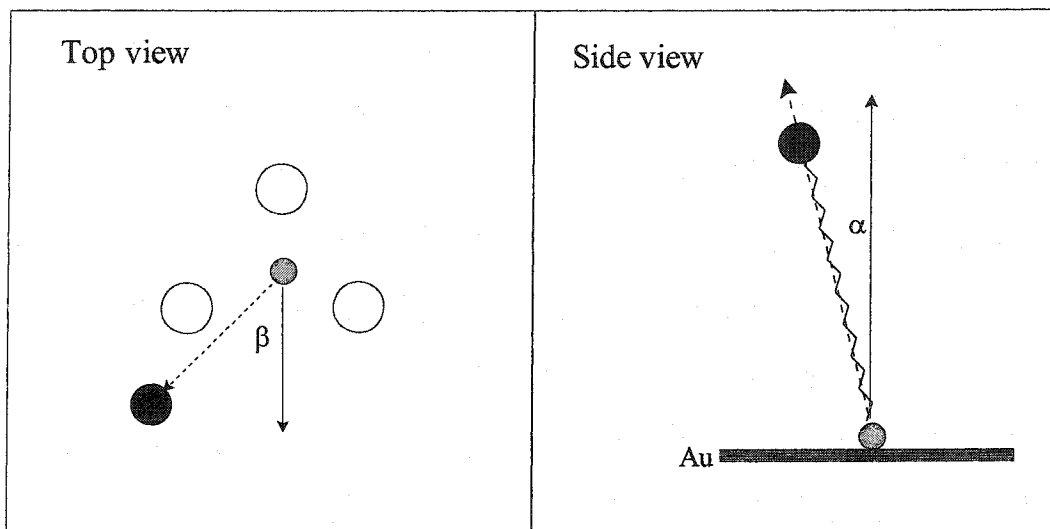


Figure 2.4. Assembly procedure of adsorption from solution.






-  headgroup
-  endgroup
-  Au

Figure 2.5. Schematic diagram of an all-trans chain orientation in an n-alkanethiols monolayer on gold surface

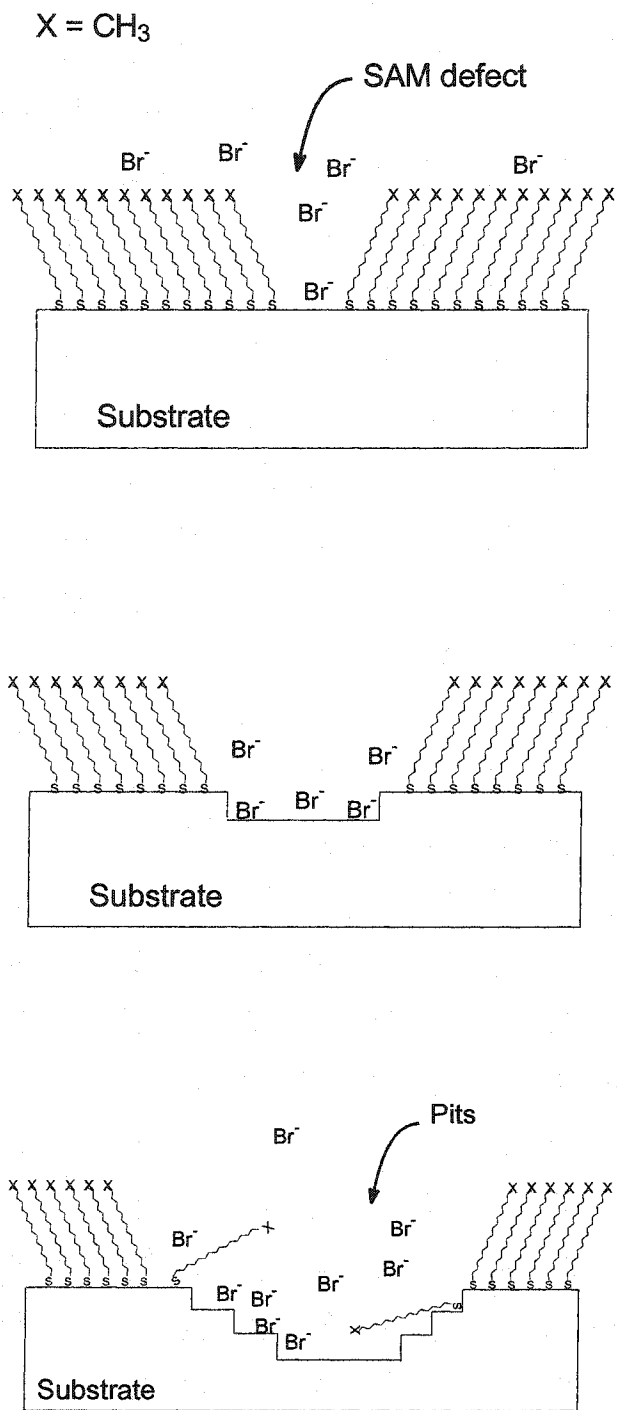


Figure 2.6. Mechanism of corrosion of SAM with hydrophobic endgroup in halide solution.

X = OH, COOH

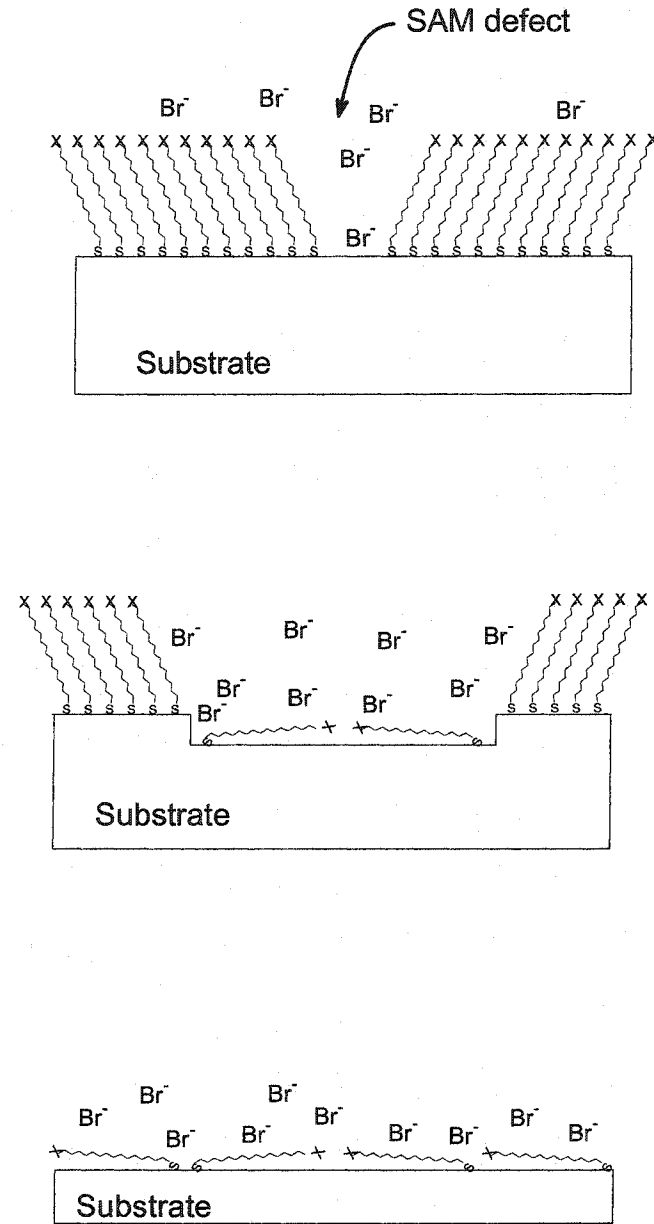


Figure 2.7. Mechanism of corrosion of SAM with hydrophilic endgroup in halide solution.

Chapter 3 Experimental Section

3.1 Chemicals

1-hexanethiol (C6SH) (Aldrich, 95%), 1-dodecanethiol (C12SH) (Aldrich, > 98%), 1-octadecanethiol (C18SH) (Aldrich, 98%) and benzyl mercapto (PhCH₂SH) (Fluka ≥ 99%) were used as received. Three alkanethiols and benzyl mercapto were dissolved in the anhydrous ethyl alcohol (Aldrich) to form 1 mM ethanolic solutions.

ACS reagent grade hydrochloric acid (Fisher), sodium chloride (Fisher), sulfuric acid (Fisher), and nitric acid (Aldrich) and deionized water were used to prepare the 0.2 M HCl, 0.2M NaCl, 0.2 M H₂SO₄, and 7 M HNO₃ solutions respectively.

3.2 Preparation of Copper Electrodes

One copper rod of 3.1 mm in diameter (Aldrich, 99.999%) was used for electrochemical experiments. The copper rods were embedded in an epoxy resin mould, leaving only their cross-section exposed to the alkanethiol alcoholic solutions and corrosive electrolyte solutions.

3.3 Monolayer Self-Assembly

The copper electrode surface was ground with SiC abrasive papers of decreasing particle size to 600 grit finish. After grinding, the sample was first rinsed with deionized water then degreased with acetone, dried in a stream of

compressed air, and then galvanostatically reduced in 1 M HClO₄ for 5 minutes, followed by etching in a 7 M HNO₃ solution for 30 seconds to obtain a fresh, oxide-free copper surface. After etching, the sample was rinsed again with deionized water and anhydrous ethanol, and finally immersed in 1 mM deoxygenated alkanethiol ethanolic solutions for 30 min - 4h, depending on the experimental requirements. The alkanethiol solution was purged with high-purity nitrogen for several hours before and during the sample immersion.

3.4 Electrochemical Measurements

All the electrochemical measurements were carried out in a conventional three-electrode cell at room temperature ($22^{\circ}\text{C} \pm 0.2$) by using a Solartron electrochemical workstation. During the measurement a bare copper electrode or one of the SAMs-covered copper electrodes was connected as the working electrode. The counter electrode was a long coiled platinum wire and the reference electrode was a saturated calomel electrode (SCE) to which all the potentials in the paper are referred. The SCE was led to the surface of the working electrode through a salt bridge with a Luggin capillary.

(i) Cyclic voltammetry.

Cyclic voltammetry was conducted for a bare copper electrode and SAMs-covered copper electrodes in 0.2 M HCl and 0.2 M NaCl solutions. Changes in current density with potential were measured from a negative initial potential to a positive vertex potential designated, and then from the positive vertex potential to

a given negative vertex potential, and finally back to the initial potential at a scan rate of 20 mV/s.

(ii) *Polarization measurements.*

The samples were immersed in the test solution till a steady open-circuit potential was reached before starting the potentiodynamic polarization measurements. The potentiodynamic polarization measurements were begun from the cathodic to the anodic potentials at a scan rate of 0.2 mV/s over a potential range of $E_{oc} \pm 150$ mV, where E_{oc} is the open-circuit corrosion potential of the electrode.

(iii) *Impedance measurements.*

EIS measurements were performed by using a Solartron 1255B frequency response analyzer interfaced to a 1287 electrochemical interface. EIS measurements were done at the open-circuit potentials, anodic or cathodic potentials in the frequency range from 60 kHz to 10 mHz with ten points per decade under the excitation of a sinusoidal wave of ± 5 mV amplitude. The impedance data were analyzed with Zview software and fitted to the appropriate equivalent circuits. The values of the elements in equivalent circuits were then derived from the fitted results.

(iv) *Electrochemical noise measurement.*

Electrochemical voltage and current noise were measured at open-circuit potentials. Two identical copper rods embedded in an epoxy were connected to a Solartron 1287 electrochemical interface, which served as a zero resistant

ammeter (ZRA) to ensure zero potential difference between the two electrodes throughout the test.

3.5 FTIR measurements

FTIR measurements were made using a Bio-Rad Digilab FTS-40 spectrometer equipped with a Harrick Scientific Seagull reflection accessory and a liquid-N₂ cooled MCT detector. Before FTIR measurements, the potential of the sample was scanned positively to a specific potential at a rate of 20mV/s. The sample was pulled out, rinsed first with deionized water then with anhydrous ethanol, and dried in a stream of compressed N₂.

3.6 Scanning Kelvin Probe Experiments

A scanning Kelvin probe was used to measure the electron work function (EWF) of the different sample surfaces. To achieve the same surface roughness, the surface of the copper samples was polished with 0.5 μm Al₂O₃, rinsed with deionized water, degreased with acetone, dried in a stream of compressed air, and then galvanostatically reduced in a 1 M HClO₄ solution for 20 minutes, to obtain oxide-free copper surface. To minimize the contamination and oxidization of SAMs, the samples were immediately transferred to the chamber where the scanning Kelvin probe experiments were performed. The measurement was performed by applying a DC potential, termed the backing potential (V_b), to the sample and detecting the output signal via an amplifier connected to the tip electrode. A data acquisition system was used to measure the average peak-to-

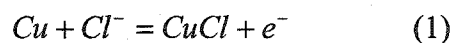
peak height (V_{ptp}) over a number of cycles as a function of V_b . The fractional changes in capacity and, thus, the work function were determined from the data set (V_{ptp} , V_b). The process of the measurement was controlled via a computer. In the present work, the reference electrode was Au, and the EWF measurements were carried out in the atmosphere.

Chapter 4. Results and Discussion

4.1 Voltammetric Characterization

Cyclic voltammograms (CVs) of the first through third scans of bare copper at 20 mV/s in 0.2 M NaCl solution are shown in Figure 4-1.

The three scan curves, similar in shape and magnitude of current, revealed two oxidation peaks (A_1 and B_1) respectively at 0.13 V and 0.48 V in forward scans and an anodic hump (C_1) at about 0.01 V and one large reduction peak (point D_1) at -0.345 V in the reverse scans. The first anodic current peak (A_1) is related to the oxidation of Cu to Cu (I).^[1,2] Before the potential was increased anodically to the first peak potential, the anodic dissolution of copper proceeds via the following two-step sequence:



where CuCl_2^- is the sole anodic dissolution product of copper according to Lee and Nobe's description.^[3] At potentials near the peak potential (0.13 V), a CuCl salt film starts to build up on the copper surface. The second anodic current peak may be ascribed to the oxidation of Cu(I) to soluble Cu(II) species and the formation of cupric oxide and/or hydroxide species in the neutral electrolyte solution used here. The large reduction peak corresponds to the reduction of soluble CuCl_2^- complex and the CuCl layer on the copper surface, which has been

proved by the CVs of the copper in Figure 4-2 in which the potential was scanned between -1.0V and 0.21 V .

The CVs in Figure 4-2 show an anodic peak and a reduction peak, whose potential positions and current magnitude correspond well to the first anodic peak and the large cathodic peak shown in Figure 4-1. The reduction hump C_1 , on the other hand, is associated with the reduction of cupric to cuprous states.

Figure 4-3 and Figure 4-4 show the CVs of the copper electrodes covered by C18SH and C12SH SAMs, respectively, at the same scan rate in 0.2 M NaCl after the copper electrodes were immersed in 1 mM alkanethiol solutions for 4 hours. Comparing with the naked copper electrode, the first CVs of the SAMs-covered electrode display a distinctive difference in the polarization behavior. In addition, the effect of the SAMs on the polarization behavior of the first CV highly depends on the length of carbon chains of SAMs.

For the C18SH or C12SH-SAMs-coated electrode, a large anodic peak (B_3 in Figure 4-3 or B_4 in Figure 4-4) and a cathodic peak (D_3 in Figure 4-3 or D_4 in Figure 4-4) were observed. Additionally, small anodic peaks, A_3 and A_4 , appeared in the first forward scan curves in Figure 4-3 and 4-4, respectively. By comparing with the CVs of the copper, it is believed that oxidation process from $\text{Cu}(0)$ to $\text{Cu}(I)$ is strongly inhibited for C18SH or C12SH SAMs-covered copper surfaces, and the electro-oxidation takes place only at the defective sites of SAMs. With further increase in the applied potential, C18SH (or C12 SH) SAMs are anticipated to be stripped off gradually from the substrate surface via electrochemical desorption,^[4-6] resulting in an increase in the defective sites, and

consequently enhancing the anodic dissolution. It is also observed that the cathodic peaks (D_3 in Figure 4-3 and D_4 in Figure 4-4) in the first CVs were smaller in magnitude than that observed with the copper electrode (D_1 in Figure 4-1). However, the polarization behavior of the C18SH (or C12SH)-SAMs-covered electrode, including the shape and current magnitude of the cathodic reduction peaks, was almost the same as that for the copper electrode for the second and subsequent cyclic voltammograms. As mentioned above, this phenomenon implies that the SAMs are removed from the copper substrate during the first cyclic voltammetric sweeping.

To confirm the strip of SAMs at the large anodic potential peak, B_3 , a separate experiment was performed by limiting the scan potential slightly below the large anodic potential.

Figure 4-5 shows that, when the C18SH-SAMs-coated electrode was repeatedly scanned in the potential region where the first anodic and the large cathodic peak appeared, both the anodic peak current and the cathodic peak current increased with the increasing scanning cycles. This observation indicates that the defects in the C18SH SAMs gradually increase with repeated potential scans even though the upper potential limit is relatively low, about 0.02 V (vs. SCE).

For the C6SH SAMs, a substantial inhibition of the electro-oxidation of the copper substrate was observed, as shown in Figure 4-6. However, its protective ability is poorer compared with C18SH-SAMs or C12SH-SAMs. The first CVs of the C6SH monolayer-covered electrode exhibited a distinct anodic

peak (A_6), which can be attributed to the oxidation of elemental copper, Cu(0), to Cu(I) species, a complex anodic peak comprised of two anodic peaks (B_6), and a cathodic peak (D_6), which is almost independent of scanning cycles. This characteristic indicates that C6SH SAMs contain more defects than C18SH or C12SH SAMs, and offer less effective inhibition to the oxidation of Cu(0) to Cu(I). It is also noticed that the cathodic peak obtained in the first scan is approximately the same in shape and current magnitude as that of the copper. This observation further supports the suggestion that there exist more defects in C6SH SAMs.

4.2 FTIR Characterization

Figure 4-7A shows the *0ex situ* FTIR reflection spectrum of C18SH on a copper surface after 4h of immersion in a 1 mM C18SH ethanol solution, and Figures 4-7B-D display those of C18SH on copper after the potentials were scanned positively to different anodic potentials.

C18SH SAMs are the CH_3 -terminated SAMs and the characteristic peak positions for methyl ($-\text{CH}_3$) and methylene ($-\text{CH}_2-$) are marked in the IR spectra. As shown in Figure 4-7A, the bands at 2963.9 cm^{-1} and 2878.8 cm^{-1} are assigned to the asymmetric (ν_a) and symmetric (ν_s) CH_3 modes, respectively; the bands at 2918.9 cm^{-1} and 2850.4 cm^{-1} are assigned to the asymmetric (ν_a) and symmetric (ν_s) CH_2 modes, respectively. The infrared reflection spectra for self-assembled C18SH on copper are similar to those of the C18SH SAMs on gold reported by Porter *et al.*,^[7] thereby further confirming that the C18SH monolayer was self-assembled successfully on the copper surface. When the potential was scanned

positively to the potential corresponding to the end of the first anodic peak (0.014 V) and the one in the rising part of the second anodic peak (about 0.30 V), the IR spectra (see Figure 4-7B and 4-7C) still displayed these four characteristic bands, indicating the existence of C18SH on the copper surface. At a more positive potential after the end of the second peak (0.85 V), the IR spectrum (Figure 4-7D) shows a flat baseline, which proves that C18SH SAMs have been completely stripped off from the copper surface. IR spectra confirm that alkanethiol SAMs are gradually removed from the copper substrate with increasing anodic potential. These observations are consistent with the observations from the cyclic voltammetric study.

4.3 Polarization Curves

Polarization measurements are usually used to evaluate the effectiveness of organic coating on corrosion inhibition.

For the copper electrode, the anodic polarization curve exhibits a linear region from -0.10 V to -0.055 V with a Tafel slope of about 0.056 V/decade, which is close to the theoretical value of 0.060 V/decade. The anodic polarization also shows an anodic current peak centered at -0.019 V, which is associated with the CuCl film formation.^[2] Earlier studies by Lee and Nobe^[3] have demonstrated that CuCl_2^- is the diffusion-limiting species in the apparent Tafel region. The reduction processes involved in this electrochemical system in NaCl electrolyte are the reduction of dissolved oxygen and hydrogen evolution at a very negative potential range. Thermodynamic data show that hydrogen evolution does not

occur at a potential higher than -0.66 V (vs. SCE). Thus, the cathodic reaction in the Cu/NaCl system is essentially the reduction of dissolved oxygen, which is also controlled by the diffusion process.^[2]

For electrodes covered by the three alkanethiol SAMs, both the anodic and cathodic currents were inhibited; however the effect is more apparent for the cathodic reactions than the anodic reactions. The cathodic currents are reduced by two orders of magnitude. These results indicate that the alkanethiol monolayers significantly inhibit the reduction of dissolved oxygen and suppress moderately the anodic dissolution of copper. It is well known that the hydrophilic mercapto groups (-SH) of alkanethiol SAMs anchor on the copper surface and the hydrophobic hydrocarbon chains constitute the ultrathin protective monolayers. The protection ability of alkanethiol SAMs against corrosion of copper may be due to the non-conducting property of the alkyl moiety in the densely packed monolayers on the copper surface.^[8] The resultant surface hydrophobicity of SAMs also contributes to corrosion protection. The hydrophobic SAM surface provides an effective barrier against the intimate contact of water with the underlying copper surface, thus retarding electron transfer across the electrode/solution interface.^[9]

The protection efficiency (PE) of SAMs was calculated by the formula given below:

$$PE(\%) = \frac{i_{corr} - i'_{corr}}{i_{corr}} \times 100 \quad (3)$$

where i_{corr} and i'_{corr} denote the corrosion current densities of the bare and SAMs-coated electrodes, respectively. The corrosion current densities for all the electrodes tested were determined from the polarization curves by the Tafel extrapolation method. The values of i_{corr} or i'_{corr} , together with the corresponding values of the protection efficiency for the three SAMs, are listed in Table 4-1.

It is seen from Table 4-1 that SAMs have quite high protection efficiencies for copper corrosion, over 99%, which is in approximate agreement with Feng and co-worker's result^[9] and is much higher than the results reported by others.^[10-13] The discrepancies in protection efficiency probably arise from the surface treatment of samples before monolayers are self-assembled. Because copper, unlike gold, gets oxidized readily in the atmosphere, pretreatment of the copper surface has a significant influence on the formation of an alkanethiol SAM. The method of removing the oxides on the copper surface and the method of preventing the copper from being oxidized are the key steps for the preparation of alkanethiol SAMs. Usually, the copper surface is reduced at cathodic potentials in strong acidic solutions, such as HClO_4 , to remove the oxides on the copper surface. However, our experiments have proved that it is more important to maintain the copper surface fresh and oxide-free than to simply convert the oxides from the copper surface. Provided that in our tests the copper surface was etched in concentrated HNO_3 for 20 seconds before self-assembly of alkanethiols, the SAMs prepared this way would yield high protection efficiencies in corrosive solutions.

The significant protection ability of alkanethiol SAMs to the underlying copper and its convenient preparation methods provide a great potential of application in the corrosion protection of metals.

We will focus on investigation of electron transfer across the SAMs and the durability of SAMs in corrosive solutions in the next section.

4.4 EIS Results

4.4.1 EIS Evaluation on SAMs in corrosive solutions

Figures 4-9 through 4-11 show the Nyquist impedance plots of the bare and alkanethiol-SAMs-covered copper electrodes in 0.2 M NaCl, 0.2 M HCl and 0.2 M H₂SO₄ solutions, respectively.

The common feature of Nyquist plots for the copper electrode is that they display a small semicircle in the high-frequency region and a straight line in the low-frequency region (see Figures 4-9A, 4-10A and 4-11A). To note that, for a Cu/HCl system, the high-frequency semicircle is so small that it is almost covered by the straight line. The high-frequency semicircle is generally associated with the electrical double-layer relaxation since the charging and discharging process is rapid.^[8, 14, 15] The low-frequency straight line, *i.e.* the Warburg impedance, is attributed to diffusion of soluble reactant or product species. In chloride-containing solutions, corrosion reactions on a copper surface consist of the anodic dissolution of copper and the reduction of the dissolved oxygen, and the two reactions are believed to be diffusion controlled.^[3, 16] We are inclined to think that the diffusion of dissolved oxygen is a rate-controlling step during the

corrosion of copper. For copper corrosion in sulfuric acid, only the reduction of the dissolved oxygen involves the diffusion process. Accordingly, the Warburg impedance in Figure 4-11A is naturally ascribed to diffusion of oxygen from the bulk solution to the copper surface. The impedance spectra composed of a semicircle and a Warburg impedance can be fitted by the equivalent circuits A or B in Figure 4-12. R_s is the solution resistance between the working electrode and reference electrode, and R_t the charge transfer resistance for the corrosion reactions. In Figure 4-12A, C_{dl} is the double-layer capacitance at solution/copper interfaces, while in Figure 4-12B, a constant phase element (CPE) is substituted for the capacitor to fit more exactly the depressed semicircle. Admittance and impedance of a CPE are, respectively, defined as

$$Y_Q = Y_0(j\omega)^n \quad (4)$$

and

$$Z_Q = \frac{1}{Y_0}(j\omega)^{-n} \quad (5)$$

where subscript Q represents a CPE, Y_0 is the modulus, ω the angular frequency and n the phase.^[17]

When the copper surface was covered with the alkanethiol monolayers, the impedance behavior of the copper electrode changed significantly in both size and shape. The previous Warburg impedance observed in Figures 4-9A, 4-10A and 4-11A disappeared, and large capacitive loops, whose diameters depended on the solutions used, were observed. It is worth noticing that their low-frequency impedance behavior is very peculiar, quite different from the usual inductive

loops. The low-frequency loops obtained in chloride-containing solution appear to be similar to the inductive loops but in fact they are not since the impedance data in the low frequency are positive rather than negative. A similar behavior was also found in 0.2 M H₂SO₄ solution for the C6SH-SAMs-covered electrode (see Figure 4-11B).

As mentioned earlier, if the SAMs are defect-free insulators and strong enough to resist corrosion attack by the corrosive ions, the equivalent circuit for the SAMs-covered electrode should be a series combination of a solution resistor (R_s) and a capacitor (C_{sam}), which represents the capacitance of SAMs (Figure 4-13A), whose impedance display in the complex impedance plane should be a straight line normal to the real axis (see Figure 4-13B).

In fact, recent results^[18] have shown that electrons can penetrate SAMs even though they are defect free; moreover, the SAMs often contain molecule-sized defects.^[19-22] As a result, the impedance spectra for the SAM-covered electrodes give a slightly depressed semicircle at high frequency. Zamborini and Crooks proposed a corrosion mechanism for the electrode coated by the defect-containing SAMs.^[20] The corrosive ions, such as halide ions, can permeate the SAMs through the defect sites and directly contact the surface of bare metal, giving rise to the corrosion of metal substrate and leading to destruction of the SAMs. Long hydrocarbon chains within SAMs can partially heal the defects. It is inferred that, the whole electrode process at SAMs-covered copper electrode involves not only the electrochemical corrosion reactions at the defect sites, the transfer of electrons across the monolayers by means of the tunneling effect^[18]

and the ion/water migration within the SAMs,^[23] but also the local breakdown and self-reparation of SAMs.^[9] The peculiar low frequency impedance behavior shown by Figures 4-9B, 4-10B and 4-11B may be associated with these various features.

In general, for the metal electrodes without coatings, the diameter of the high-frequency semicircle is treated as the charge-transfer resistance (R_t),^[15] which may be used to evaluate the corrosion rate of metals and the inhibition efficiency of inhibitors against corrosion of metals. The smaller the R_t , the faster the corrosion reaction proceeds. But for the electrodes with coatings, the high frequency capacitive loop is related to the barrier and protective properties of the coatings,^[24] whereas the time constant originating from the Faradaic reactions usually appears only in low frequency because the time constant is relatively large. Different equivalent circuits^[23, 25, 26] have been established so far to interpret impedance behavior of the SAMs-coated electrodes. However, these circuits are inconsistent with each other in interpreting the physical meaning of elements and explaining the origin of the high-frequency semicircle. In this study, we consider that SAMs behave somewhat like organic coatings, on the basis of Deflorian and co-workers' model for protective coatings,^[24] a general equivalent circuit for a SAMs-covered electrode is established (see Figure 4-14A).

In Figure 4-14A, R_s , R_t , C_{dl} and Z_w have the same physical meaning as in Figure 4-12A; C_{sam} is the capacitance of the SAMs, R_{sam} represents the transfer resistance of electrons through the monolayers, which reflects the protective properties of the SAMs. If CPEs are used to replace the capacitive elements, the

improved equivalent circuit is shown in Figure 4-14B. When the influence of the mass transport process is insignificant, Z_w can be ignored and the equivalent circuit in Figure 4-14 B can be simplified to the one in Figure 4-14C. The circuit in Figure 4-14B can be further simplified to the circuit in Figure 4-14 D under the condition that $R_{sam} \gg R_t$.^[9]

The impedance spectra for the copper electrodes of bare and coated with the SAMs were fitted by using circuit B in Figure 4-12 and circuit D in Figure 4-14, respectively. Here we just fitted the high-frequency capacitive loops of the SAMs-covered copper (see solid lines in Figures 4-9 through 4-11). The values of elements of equivalent circuits obtained by fitting are given in Table 4-2. The capacitance values of SAMs and the double-layer were calculated by means of the method proposed by Ma^[17] and are also listed in this table.

Comparison of values of R_{sam} and C_{sam} for C18SH, C12SH and C6SH monolayers shows that the longer the hydrocarbon chain, the larger the value of R_{sam} and the smaller the value of C_{sam} . The quality of SAMs can be evaluated by R_{sam} and C_{sam} . In general, the more densely packed the monolayers and the thicker the monolayers, the higher the R_{sam} values and the lower the C_{sam} values. It is evident that the long hydrocarbon chain is favorable for the corrosion protection of SAMs. In corrosion studies the n value of a CPE reflects the roughness of the electrode surface.^[1] In the case of a perfectly smooth electrode, n would have a value of +1. We noticed that n values of the Q_{dl} element describing the double-layer of copper in NaCl, HCl and H₂SO₄ solutions are 0.66, 0.49 and 0.80, respectively. The deviation from a value of unit is ascribed to the surface

roughness of the copper electrode caused by corrosion, whereas most n values of the Q_{sam} element are over 0.90. The high value of n results from the fact that the electrode surface modified by alkanethiol SAMs was kept smooth due to reduced corrosion.

In view of the order arrangement of alkanethiol SAMs on gold, silver and copper surfaces, the capacitive behavior can be described approximately by the Helmholtz model of the double-layer although the model is rather simplified. Taking the C6SH SAM on copper as an example, if the SAM acts as an ideal capacitor, the capacitance per unit area is:

$$C = \epsilon\epsilon_0 / d \quad (6)$$

where d is the thickness of the C6SH monolayers, ϵ_0 is the permittivity of vacuum, a fundamental constant with the value $8.854 \times 10^{-12} \text{ C}^2 \text{ J}^{-1} \text{ m}^{-1}$, and ϵ is the relative permittivity. Based on the data reported by Lange's Hand Book of Chemistry,^[27] the length of a C-C bond is about $1.541 \times 10^{-10} \text{ m}$ and that of C-S bond is $1.817 \times 10^{-10} \text{ m}$. It is roughly estimated that the length of a C6SH molecule is $0.7 \times 10^{-9} \text{ m}$, which is treated approximately as the thickness of a C6SH monolayer. The relative permittivity of ethylmercaptan (6.9) was used as the reference value of C6SH. With these values, the capacitance of the C6SH SAMs is calculated to be about $3.5 \times 10^{-2} \text{ F m}^2$, *i.e.* $3.5 \mu\text{F cm}^{-2}$. Within the errors of experiment and theoretical treatment, this value can be considered to be in good agreement with the values listed in Table 4-2, thereby confirming that the

equivalent circuits for the SAMs-coated electrode are creditable and the analysis and treatment for impedance data are reasonable.

4.4.2 EIS Evaluation on Formation Process of C12SH SAMs.

The C12SH monolayers were formed on copper by immersing the copper electrodes in 1 mM C12SH solution in absolute ethanol for varying times. Figure 4-15 gives the Nyquist impedance spectra for the electrode covered by C12SH monolayers in 0.2 M NaCl solution at the open-circuit potentials. When the formation times of monolayers were short (0.5h, 1h), the corresponding impedance spectra displayed the obvious Warburg impedance. This implies that the C12SH monolayers are not sufficiently dense to completely block the corrosion reactions at the whole copper substrate. But after 2 hours of immersion in C12SH solution, the low-frequency impedance behavior greatly changed and the impedance spectrum evolved into the one diagram composed of two capacitive loops. The high-frequency capacitive loop arises from the transfer of electrons in SAMs through the tunneling effect,^[18] and the low-frequency loop is ascribed to the relaxation of the double layer according to the equivalent circuit in Figure 4-14B. In this case, the C12SH monolayers are improved in the compact and orderly properties, but still have some defects through which the corrosion reactions take place at the bare substrate. With further increasing self-assembling time, the C12SH monolayers on copper become denser and more ordered and the defective sites are healed and repaired by the long hydrocarbon chains.^[9] The impedance spectrum after 4 h of immersion shows a near-regular semicircle with

a larger diameter, which indicates the corrosion reaction is significantly inhibited. The evolution of the high-frequency capacitive loop with the self-assembling time reflects the improvement of SAMs in terms of ordered state and compact structure. Using the equivalent circuit shown in Figure 4-14D to fit the high-frequency capacitive loop, the variations of Y_0 and n of Q_{sam} with the immersion time are plotted in Figure 4-16. It is found from Figure 4-16 that the longer the immersion times, the smaller the Y_0 values and the higher the n values. Variation of n with the immersion time, *i.e.*, n approaching unity, indicates that the C12SH monolayer tends to behave like a perfect capacitor. The dependence of Y_0 on the self-assembling time can be interpreted in terms of Equation (7). Y_0 may be treated simply as the capacitance here since the value of n is approaching 1.

$$C_t = C_{sam}(1 - \theta) + C_{dl}\theta \quad (7)$$

where C_t is total capacitance of an electrode partially covered by SAMs, C_{sam} is that of the SAMs, C_{dl} is the capacitance of the double-layer at bare sites on the electrode surface, and θ is the area fraction of the bare sites. In Equation (7), $C_{sam} \ll C_{dl}$. Thus, the C_t value will gradually decrease with increasing SAMs' formation times because of decreasing θ with the formation time.

4.4.3 The Destruction of C12SH SAMs in NaCl

Figure 4-17 shows a group of impedance spectra for the copper electrode covered by C12SH monolayers in 0.2 M NaCl solution at the open-circuit potentials. With increasing exposure time to NaCl solution, the high frequency capacitive loop gradually decreased in size and the Warburg impedance appeared

in the low frequency. This kind of changing trend, contrary to that shown in Figure 4-15, reveals that the corrosion protection ability of the SAMs decreases with the immersion time. Theoretically, the defect sites in SAMs are attacked by the corrosive ions at first, followed by extension of defect sites, leading to the local breakdown of SAMs. The capacitive loops were fitted by the equivalent circuit in Figure 4-14D and then Y_0 and n of Q_{sam} were plotted as functions of the immersion time (see Figure 4-18), following the method described above. Figure 4-18 shows that n decreases but Y_0 increases with the immersion time in the NaCl solution. The decrease in the n values is related to the increase of surface roughness of the electrode, and the increase of Y_0 values should be attributed to the increase of θ according to Equation (7).

4.4.4 Stability of Alkanethiol SAMs as a Function of Applied Potential

The dependence of capacitance of SAMs on the applied potential is measured, from which the development of defects in the SAMs can be detected. The capacitance value measured at different potentials is the electrode capacitance of the SAMs/solution interface, including the capacitance of SAMs and that of the electric double-layer, whereas the electrode capacitance is dependent on both frequency and the applied potential. Therefore, selecting an appropriate frequency to deduce the contribution of the double-layer capacitance is the key in measuring the capacitance-potential curves. After repeated attempts we have found that the

top frequency of the high frequency capacitive loop is the optimum frequency to carry out these experiments.

Figure 4-19 shows three curves of capacitance vs. the applied potentials for the C12SH-SAMs-coated copper electrode. In the case of short self-assembling time the capacitance value decreased at first and then increased with the potential (curve A). The relatively high capacitance values reveal that they include a great contribution from the double layer capacitance. As mentioned earlier, at short immersion time, there exist some defects in the C12SH SAMs where the corrosion reactions occur at the bare copper substrate; moreover, the applied potential induced further development of the defects. The capacitance-potential curve (B) for the electrode coated by SAMs assembled for 2 hours was similar to curve A, but the value of capacitance decreased by one order of magnitude. With further extending the self-assembling time, on the one hand the capacitance values continued decreasing; on the other hand, the capacitance increased monotonously with the increase of potential without a minimum capacitance (curve C). This implies that the defects of SAMs have been repaired with the extended self-assembling time. In this case, the SAMs remain stable at the cathodic polarization potential. Small capacitance values at the cathodic polarization potentials somewhat confirm the significant cathodic inhibition of SAMs. It is worth noticing that the electrode capacitance rapidly increases with increasing potential, which may be attributed to the defect extension in SAMs caused by the electrochemical desorption of SAMs at anodic potentials. These results are in agreement with cyclic voltammetric and polarization results.

4.5 Measurements of Electrochemical Noise (EI)

Pitting corrosion is one of the most destructive forms of corrosion among varieties of corrosion. In the mid-1980's Smialowska summed up five types of pitting and characterized the features of each type. The most common and most important type of pitting occurs on the passivated iron base alloys in contact with halide-containing aggressive solutions, which involves breakdown of passive film on iron and its alloys.

The gold or copper surface modified by n-alkanethiol SAMs has been reported to suffer pitting corrosion,^[20, 28] but this kind of so-called pitting is greatly different from the conventional pitting in initiation and propagation mechanism. Its origin is related to the defects within the monolayer, where corrosive ion can attack the bare substrate and initiate local dissolution. The electrochemical Noise (EN) technique provides a good method to monitor *in situ* the pit development occurring on the SAMs-covered metal surface.

Two identical copper rod specimens were inserted in an epoxy resin mould to prepare the coupled electrodes. Electrochemical current noise is measured as the galvanic coupling current between two nominally identical working electrodes, with the current being measured using a zero resistance ammeter (ZRA) to ensure the two electrodes are at the same potential.^[29] If the two electrodes are corroded generally, the electrode reaction kinetics of the two electrodes should be approximately identical, and no net current flow between the electrodes can be detected. However, if the two electrodes suffer localized corrosion, especially

pitting attack, there should be net coupling current between two electrodes due to the difference in reaction kinetics of the electrodes. Here both current noise and potential noise were measured simultaneously.

Figures 4-20 to 4-22 display a set of plots of potential noise and current noise for a C18SH SAMs-covered copper electrode in 0.2 M HCl solution at the open-circuit potential. During the first 2000 seconds, as shown by Figure 4-20, the potential baseline gradually decreased with time increase, whereas the current baseline increased with time; small potential and current fluctuations were observed before 1700 seconds, but regular large potential and current noise signals appeared after 1700 seconds. Moreover, there is one-to-one correspondence between the potential noise signal and current noise signals. This shows the pitting corrosion began to take place. Both potential and current signals regularly change with time. Both potential and current baselines tended to stable values; on the other hand, the longer the immersion time, the more frequently the noise signals occurred (see Figures 4-21, 4-22), revealing the frequent occurrence of the initiation, growth and reparation of pits.

It is observed that the potential noise exhibits a relatively rapid rise due to the formation of metastable pitting, followed by a slow decay as the pit repassivates, and the same is true of current noise. The pits might result from the fact that the defective sites of SAMs are attacked by the corrosive ions, causing the corrosion of copper substrate; and perfect sites have not been corroded since they have a strong resistance to attack of corrosive ions. The repassivation of SAMs in corrosive solution, unlike repassivation of passive films, should be

attributed to reorientation of alkanethiols around the pits as proposed by Zamborini and Crooks.^[20] Long hydrocarbon chains within SAMs can partially heal the defects. It is of interest that both positive and negative current noise signals were observed. The initiation, growth and death processes of pits occur consecutively on the two SAMS-covered copper surfaces. The coupling current between the two nominally identical working electrodes also therefore changes in direction at different times, sometimes positive and sometimes negative.

For the coupled copper electrodes free of SAMs, no regular electrochemical noise signals have been observed in the same solutions except small irregular current or potential fluctuations. This fact indicates that the bare copper surface suffers general corrosion rather than pitting. This is the first time we report the pitting corrosion studies by means of EN techniques. Much experimental works and theoretical interpretation is ongoing.

4.6 Scanning Kelvin Probe (SPK)

The Kelvin probe method is a powerful tool for the study of electric properties of surface as well as for determination of surface parameters. Lü *et al.* performed a series of studies on the local contact potential of n-alkanethiol SAMs on Au by Kelvin probe force microscopy.^[30, 31] Their results show that the surface potential increases with increasing chain length of thiols, which is similar to Evan's observation. Furthermore, the authors have demonstrated that the Kelvin probe technique can provide good resolution even under ambient pressure, thereby greatly broadening the application range of the Kelvin probe.

Anodic dissolution of metal involves the electron transfer at the metal/solution interface. Therefore, for the copper electrodes covered by SAMs, the degree of ease for an electron to escape from the Fermi level to the free electron state which is characterized by the electron work functions (EWFs) reflects the chemical stability and the protective ability of the SAMs. In this work, a scanning Kelvin probe was used to determine the EWFs of the copper surface for two samples, one C12SH SAMs-covered copper electrode and one PhCH₂SH SAMs-covered copper electrode. During these tests, an area of 40 μ m \times 40 μ m was scanned. Figure 4-23 presents EWFs of the surface of two electrode samples. EWF of the C12SH SAMs-covered copper surface is lower than that of PhCH₂SH SAMs-covered copper surface. As EMFs are related to the electron transfer across SAMs, the values of EMFs might reflect the protective properties of SAMs. On the other hand, the smoother the potential surface, the more homogeneous the SAMs and the fewer the defects of SAMs. It seems that the SAMs are not so homogeneous as expected. C12SH SAMs appear to be more densely packed with fewer defects, compared with PhCH₂SH (benzothiol) SAMs. The possible reason is that the rigid, bulk unit of the benzene ring in the SAMs cannot cover the copper surface more effectively than the flexible alkyl chains of n-alkane have done. The latter can form densely compact and ordered monolayers.

4.7 Summaries

The self-assembled C18SH, C12SH and C6SH monolayers (SAMs) on copper provide significant corrosion protection for underlying copper in different aggressive medium, such as NaCl, HCl and H₂SO₄ solutions. The protection ability of SAMs strongly depends on the pretreatment of the copper surface. A two-step pretreatment of copper, which including cathodic reduction in 1 M HClO₄ solution and a following etching in 7 M HNO₃ solution before self-assembly yields the highest quality of SAMs formed on copper in terms of corrosion protection efficiencies. The SAMs greatly inhibit the cathodic current of copper in 0.2 M NaCl solution, giving rise to a protection efficiency of over 99%. Particularly, the SAMs inhibit more strongly the cathodic reaction than the anodic reaction. The length of hydrocarbon chains has great influence on corrosion protection of the alkanethiol SAMs. The longer the carbon chains, the better the corrosion protection efficiency of SAMs.

The cyclic voltammetric results, together with FTIR characterization, have confirmed that the alkanethiol SAMs are able to retard the electro-oxidation of copper from the Cu(0) to Cu(I) species; however, the SAMs can be stripped off from the copper substrate at more positive potentials. The cyclic voltammograms for the copper electrode covered by alkanethiol SAMs were similar to those of the copper electrode for the second and subsequent cyclic voltammetric measurements. The long hydrocarbon chains are advantageous to the anodic inhibition of SAMs.

A general equivalent circuit for the SAMs-covered electrode was proposed. The high frequency capacitive loop originates from the transfer of

electrons across the monolayers through the tunneling effect and the impedance behavior in low frequency is related to the corrosion reaction at the bare copper/solution interface. The value of capacitance of SAMs calculated by the equivalent circuit was in good agreement with the theoretical value. The n and Y_0 of the Q_{sam} element in the equivalent circuit may be used to evaluate the quality of SAMs and their defect development in corrosive solutions. The closer the n value to 1, the smaller the Y_0 value and the higher the quality of SAMs.

For the SAMs-covered electrode, the plots of capacitance vs. the applied potential offer a convenient method to determine the stability of SAMs under the applied potentials.

EN results indicate that the copper electrode coated with C18SH SAMs has suffered pitting corrosion in HCl solutions. The electrochemical noise signals might arise from the fact that the defective sites are attacked by corrosive ions at first and the hydrocarbon chains can partially heal the defects by reorientation of alkanethiols around the defects.

The Scanning Kelvin Probe provides a good tool to detect the defects within SAMs. Compared with C12SH SAMs, PhCH₂SH SAMs contained more obvious defects since the latter molecules cannot arrange orderly like the former molecules.

- [1] A. V. Benedetti, P. T. A. Sumodjo, K. Nobe, P. L. Cabot, W. G. Proud, *Electrochim. Acta* **1995**, *40*, 2657.
- [2] R. C. Thomas, L. Sun, M. Crooks, *Langmuir* **1991**, *7*, 620.
- [3] H. P. Lee, K. Nobe, *J. Electrochem. Soc.* **1986**, *133*, 2035.

- [4] Z. Bozkurt, Z. Xu, S. H. R. Brienne, I. S. Butler, J. A. Finch, *J. Electroanal. Chem.* **1999**, *475*, 124.
- [5] M. M. Abu-Omar, S. I. Khan, *Inorg. Chem.* **1998**, *37*, 4979.
- [6] J. B. Arterburm, M. C. Perry, S. L. Nelson, B. R. Dible, M. S. Holguin, *J. Am. Chem. Soc.* **1997**, *119*, 9309.
- [7] M. D. Porter, T. B. Bright, D. L. Allara, C. E. D. Chidsey, *J. Am. Chem. Soc.* **1987**, *109*, 3559.
- [8] Y. Feng, W.-K. Teo, K.-S. Siow, Z. Gao, K.-L. Tan, A.-K. Hsieh, *J. Electrochem. Soc.* **1997**, *144*, 55.
- [9] G. K. Jennings, J. C. Munro, T.-H. Yong, P. E. Laibinis, *Langmuir* **1998**, *14*, 6130.
- [10] M. Itoh, Nishihara, K. H. Aramaki, *J. Electrochem. Soc.* **1995**, *142*, 1839.
- [11] R. Haneda, H. Nishihara, K. Aramaki, *J. Electrochem. Soc.* **1997**, *144*, 1215.
- [12] Y. Yamamoto, H. Nishihara, K. Aramaki, *J. Electrochem. Soc.* **1993**, *140*, 436.
- [13] M. Ishibashi, M. Itoh, H. Nishihara, K. Aramaki, *Electrochim. Acta* **1996**, *41*, 241.
- [14] O. E. Barcia, O. R. Matoos, N. Pebere, B. Tribollet, *J. Electrochem. Soc.* **1993**, *140*, 2825.
- [15] O. E. Barcia, O. R. Matoos, *Electrochim. Acta* **1990**, *35*, 1601.
- [16] L. Bacarella, J. C. J. Griess, *J. Electrochem. Soc.* **1973**, *120*, 459.
- [17] X. Wu, H. Ma, S. Chen, Z. Xu, A. Su, *J. Electrochem. Soc.* **1999**, *146*, 1847.
- [18] T. M. Nahir, E. F. Bowden, *Electrochim. Acta* **1994**, *39*, 2347.
- [19] L. Sun, R. M. Crooks, *J. Electrochem. Soc.* **1991**, *138*, L23.
- [20] F. P. Zamborini, R. M. Crooks, *Langmuir* **1998**, *14*, 3279.
- [21] X.-M. Zhao, J. L. Wilbur, G. M. Whitesides, *Langmuir* **1996**, *12*, 3257.
- [22] O. Chailapakul, L. Sun, C. Xu, M. Crook, *J. Am. Chem. Soc.* **1993**, *115*, 12459.
- [23] E. Boubour, R. B. Lennox, *J. Phys. Chem. B* **2000**, *104*, 9004.
- [24] F. Deflorian, L. Fedrizzi, A. Locaspi, P. L. Bonora, *Electrochim. Acta* **1993**, *38*, 1945.
- [25] R. P. Janek, W. R. Fawcett, *Langmuir* **1998**, *14*, 3011.
- [26] R. P. Janek, W. R. Fawcett, *J. Phys. Chem. B* **1997**, *101*, 8550.
- [27] J. A. Dean, *Lange's Handbook of Chemistry*, 14th ed., McGraw-Hill, New York, **1992**.
- [28] J. Scherer, M. R. Vogt, O. M. Magnussen, R. J. Behm, *Langmuir* **1997**, *13*, 7045.
- [29] W. P. Iverson, *J. Electrochem. Soc.* **1968**, *115*, 617.
- [30] J. Lü, E. Delamarche, L. Eng, R. Benenwitz, E. Meyer, H.-J. Gütherodt, *Langmuir* **1999**, *15*, 8184.
- [31] J. Lü, L. Eng, R. Bennewitz, E. Meyer, H.-J. Gütherodt, E. Delamarche, L. Scadella, *Surf. Interface Anal.* **1999**, *27*, 368.

Table 4-1.

The Corrosion Current Density for the Bare and SAMs-Covered Electrodes and Protection Efficiency (PE) of Alkanethiol SAMs in 0.2 M NaCl Solution

Electrodes	$i_{corr} / \text{A cm}^{-2}$	PE / %
Bare	8.0×10^{-6}	—
C18SH-SAMs	2.04×10^{-8}	99.7
C12SH-SAMs	2.10×10^{-8}	99.7
C6SH-SAMs	3.26×10^{-8}	99.5

Table 4-2, Values of the Elements of the Equivalent Circuits in Figures 7B and 9D to Fit the Impedance Spectra for the Electrodes of Bare and Covered by Alkanethiol SAMs as Well as the Values of C_{dl} , C_a Calculated.

	$R_{sam} / \Omega cm^2$	$R_t / \Omega cm^2$	Q_{sam}	$Y_0 / \Omega^{-1} cm^{-2} s^n$	n	$Y_0 / \Omega^{-1} cm^{-2} s^n$	n	$C_{sam} / \mu F cm^{-2}$	$C_{dl} / \mu F cm^{-2}$	$W / \Omega cm^2$
0.2 M NaCl										
Bare Cu	-	1.99×10^3	-	-	-	4.22×10^{-4}	0.66	-	385.4	1.52×10^{-5}
C18SH	3.47×10^5	-	3.40×10^{-7}	0.98	-	-	-	0.33	-	-
C12SH	1.21×10^5	-	5.24×10^{-7}	0.97	-	-	-	0.48	-	-
C6SH	7.5×10^4	-	2.26×10^{-6}	0.91	-	-	-	1.90	-	-
0.2 M HCl										
Bare Cu	-	8.65×10^2	-	-	-	4.89×10^{-3}	0.49	-	2.20×10^3	4.10×10^{-5}
C18SH	1.79×10^5	-	1.92×10^{-7}	0.97	-	-	-	0.17	-	-
C12SH	1.04×10^5	-	1.29×10^{-7}	0.92	-	-	-	0.09	-	-
C6SH	6.44×10^4	-	1.68×10^{-6}	0.96	-	-	-	1.53	-	-
0.2 M H ₂ SO ₄										
Cu	-	5.49×10^2	-	-	-	1.07×10^{-4}	0.80	-	52.9	3.82×10^{-5}
C18SH	1.68×10^5	-	2.94×10^{-7}	0.93	-	-	-	0.23	-	-
C12SH	8.28×10^4	-	1.33×10^{-6}	0.92	-	-	-	0.99	-	-
C6SH	7.35×10^4	-	1.51×10^{-6}	0.97	-	-	-	1.41	-	-

Figures in Chapter 4

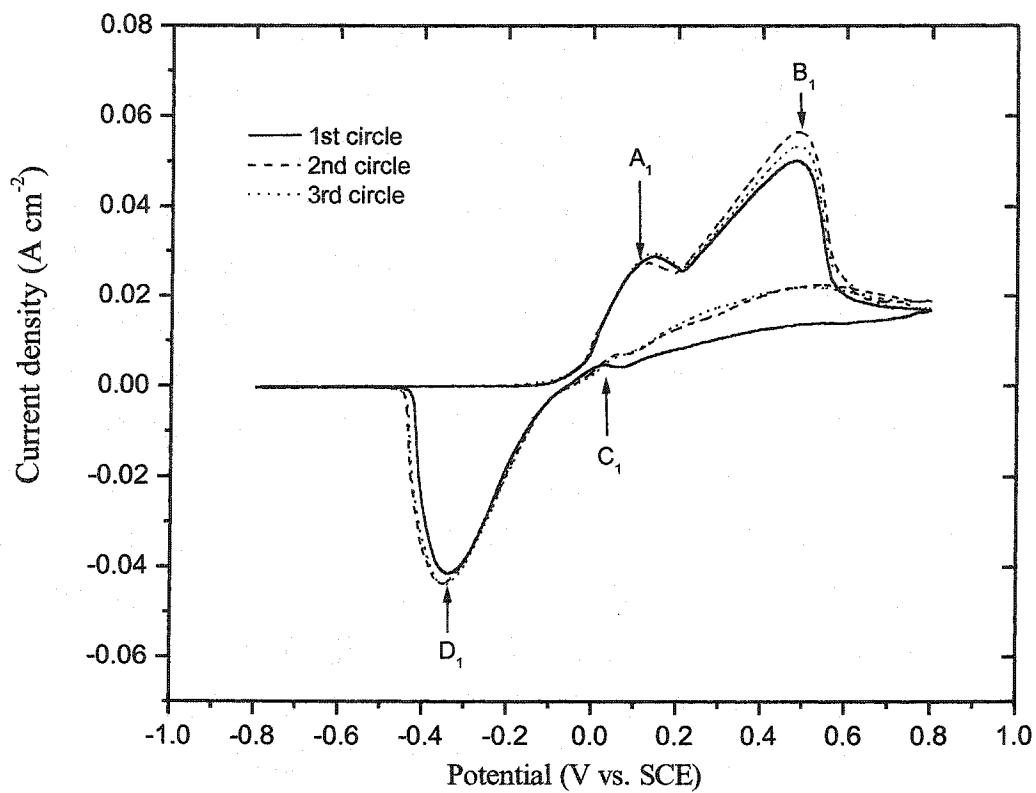


Figure 4-1. Cyclic voltammograms of bare copper in 0.2 M NaCl solution

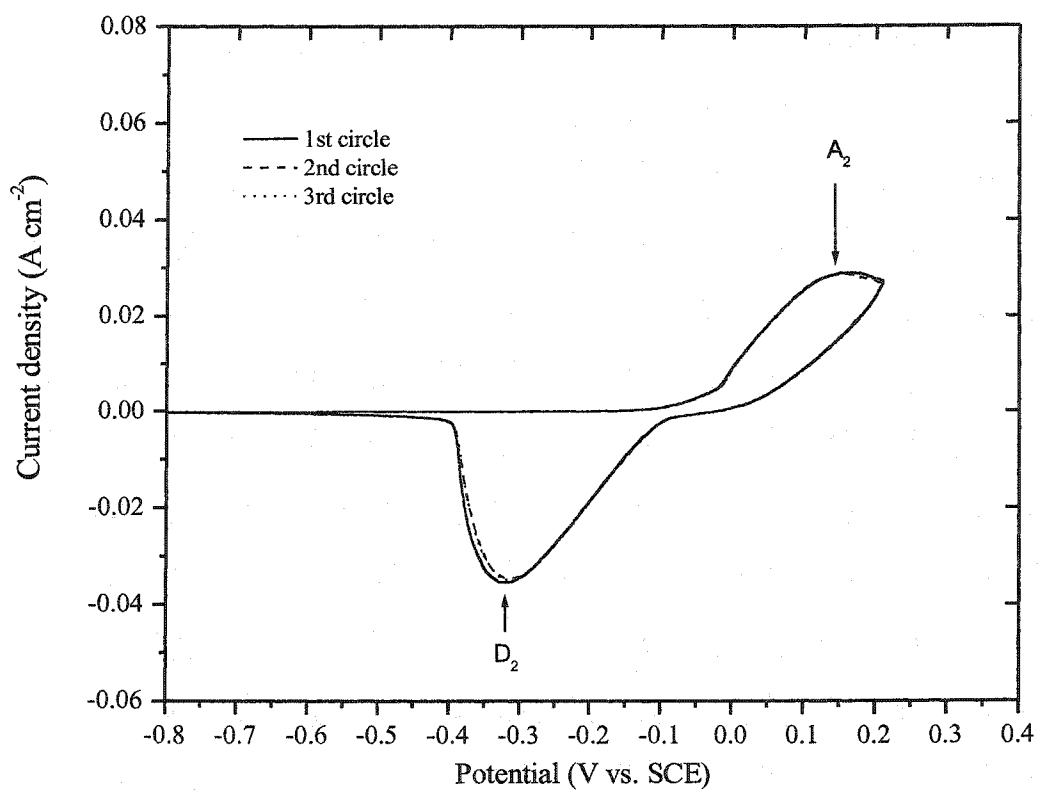


Figure 4-2. Cyclic votammograms of bare copper in 0.2 M NaCl solution

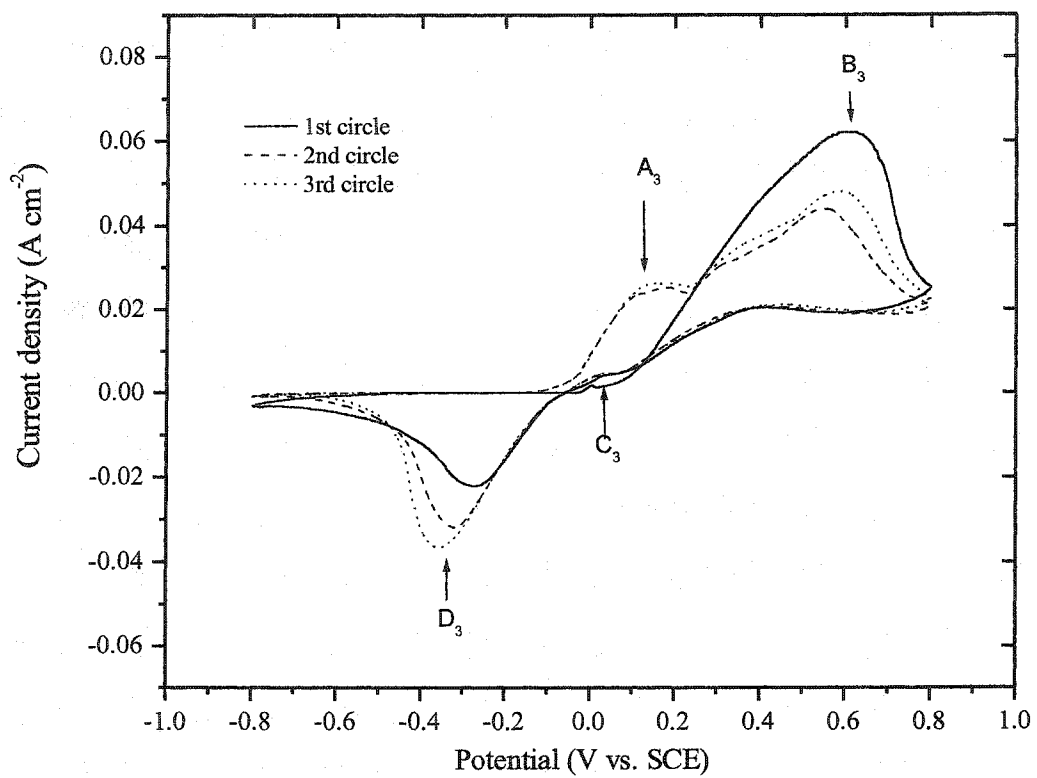


Figure 4-3. Cyclic voltammograms for C18SH-covered copper electrodes in 0.2 M NaCl solutions

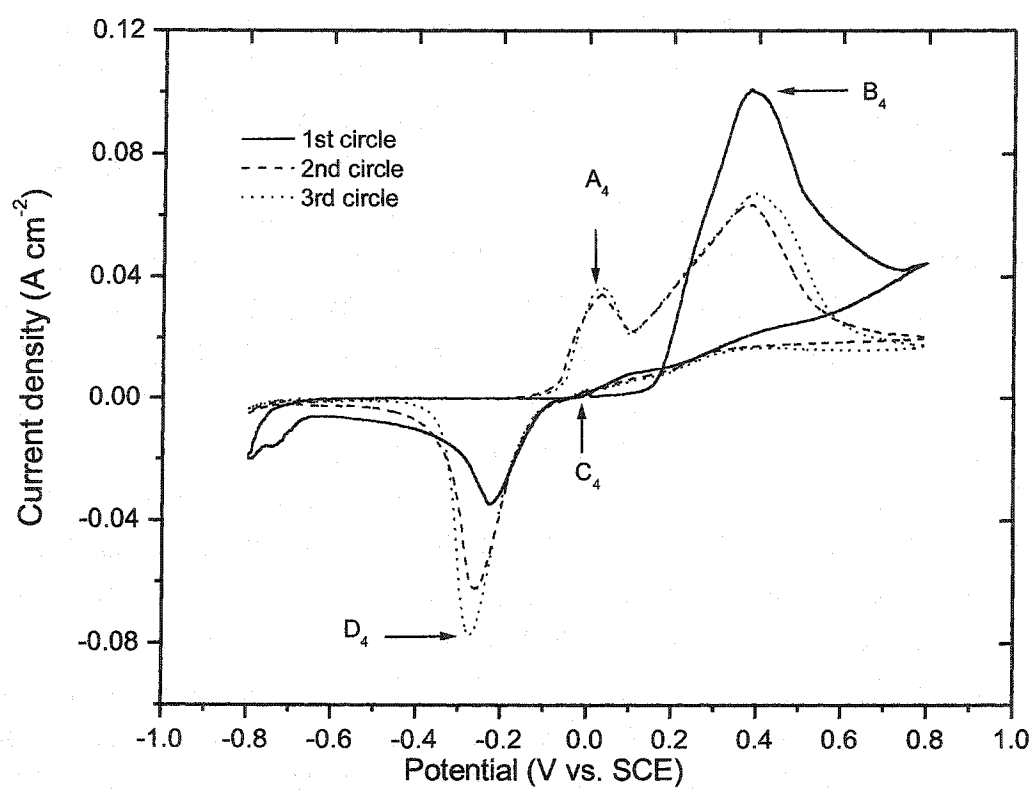


Figure 4-4. Cyclic voltammograms for C12SH-covered copper electrodes in 0.2 M NaCl solutions.

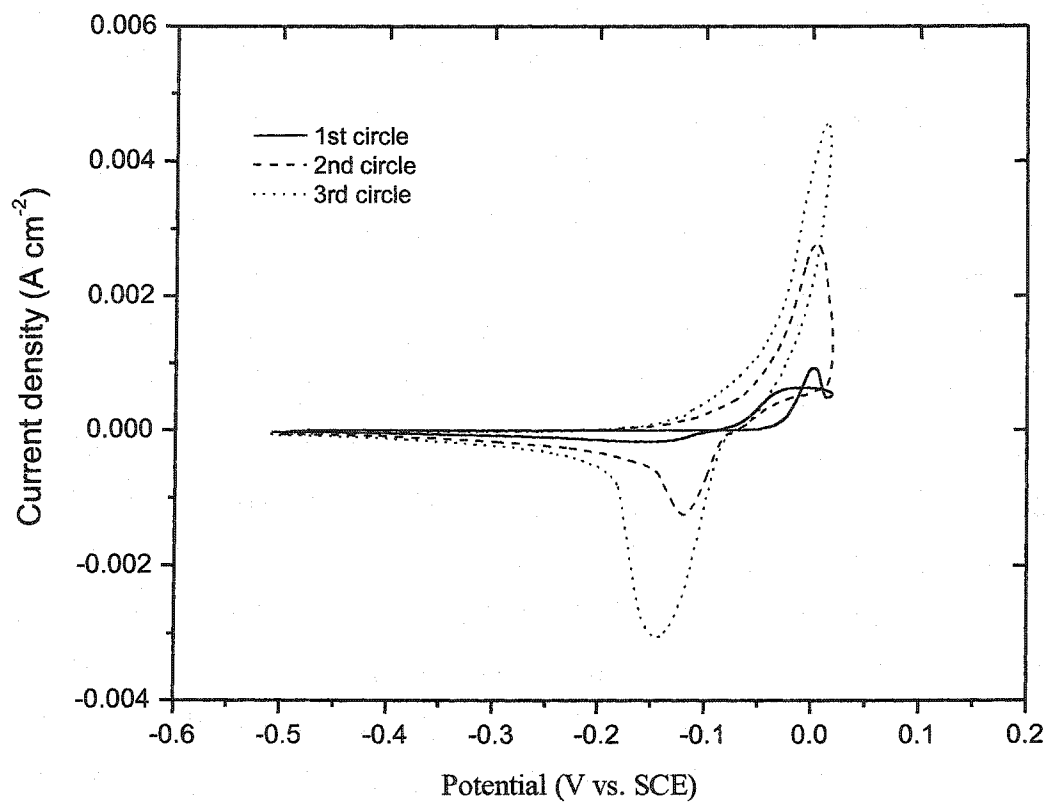


Figure 4-5. Cyclic voltammograms for C18SH-covered copper electrodes in 0.2 M NaCl solutions

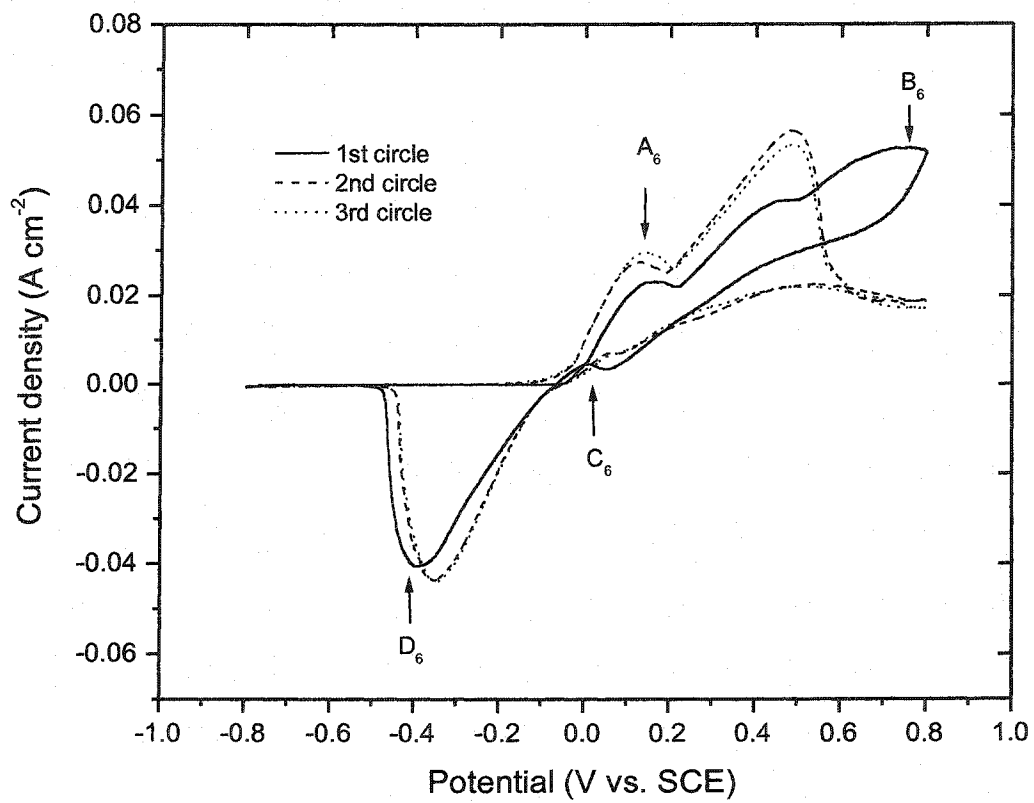


Figure 4-6. Cyclic voltammograms for C₆SH-covered copper electrodes in 0.2 M NaCl solutions

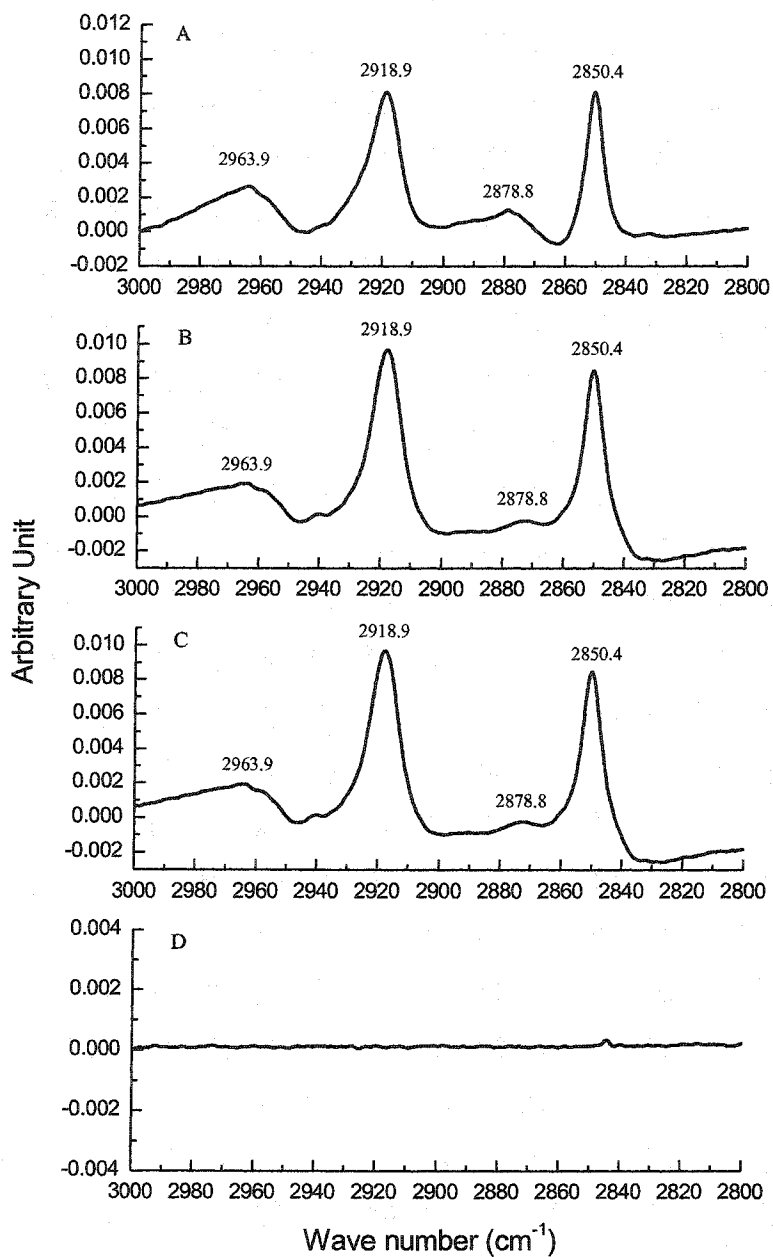


Figure 4-7. FTIR reflection spectra for the copper electrode covered by C18SH SAMs in 0.2 M NaCl solution before the potential scan (A) and at anodic potentials of 0.014 V (B), 0.30 V (C) and 0.85 V (D).

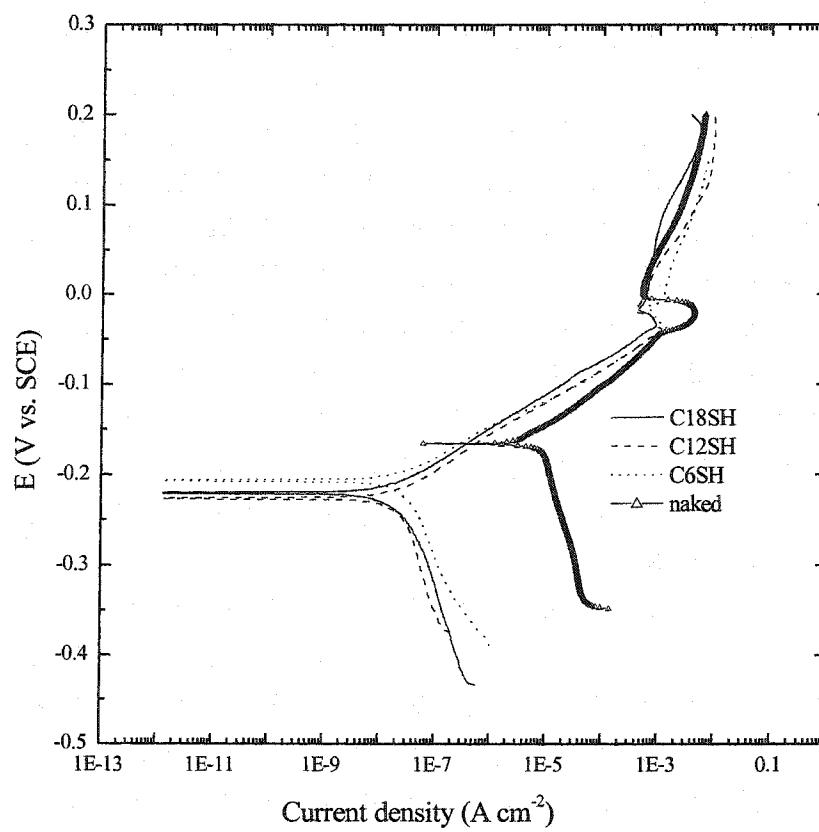


Figure 4-8. Polarization curves for the bare copper electrode and the SAMs-coated copper electrodes in 0.2 M NaCl solutions.

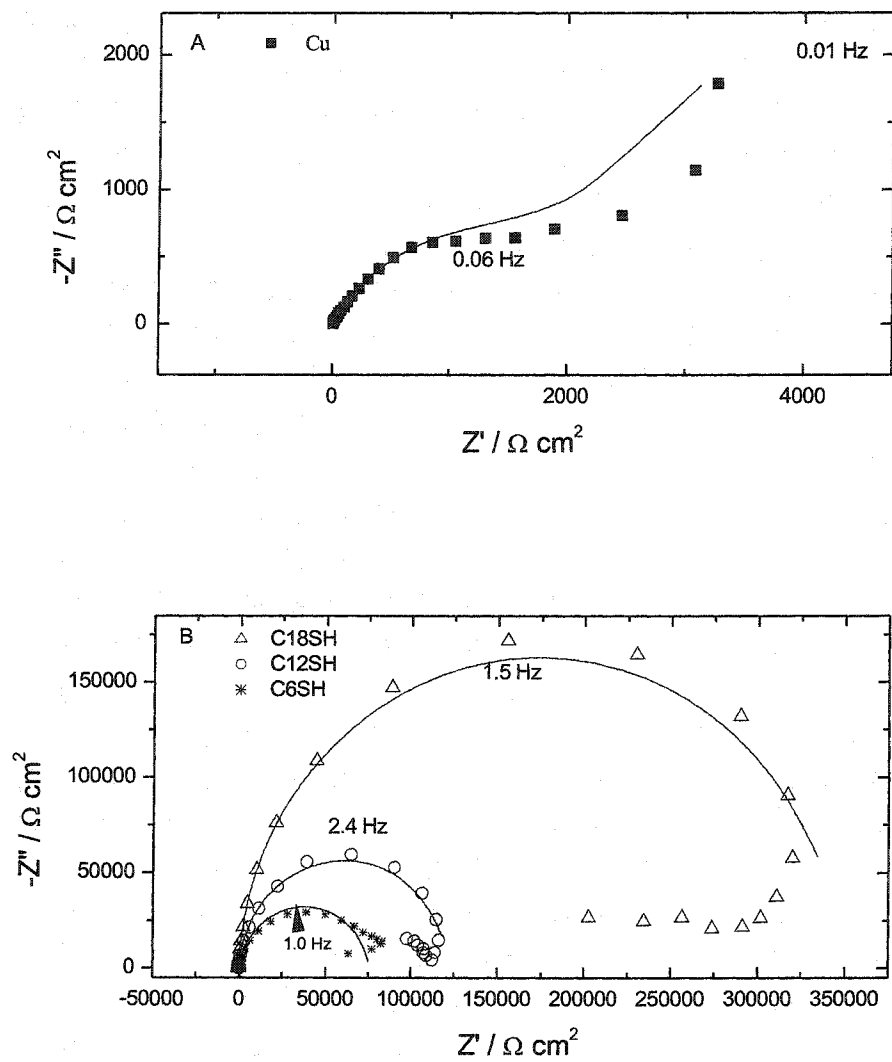


Figure 4-9. Nyquist impedance spectra for the bare (A) and alkanethiol-SAMs-covered (B) copper electrodes in 0.2 M NaCl solutions at the open-circuit potentials. Formation times of SAMs are 4h. Symbols: measured data; solid line: fitted curve.

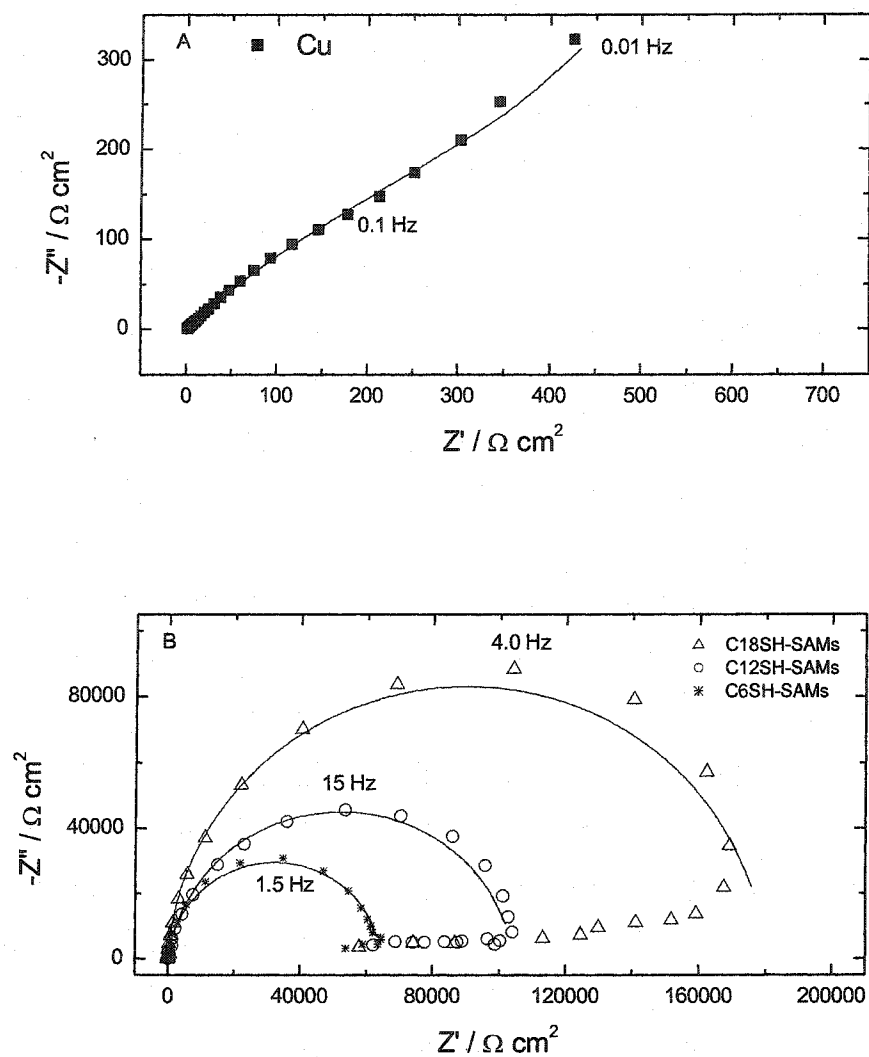


Figure 4-10. Nyquist impedance spectra for the bare (A) and alkanethiol-SAMs-covered (B) copper electrodes in 0.2 M HCl solutions at the open-circuit potentials. Self-assembling times of alkanethiol monolayers at copper are 4h.

Symbols: measured data; solid line: fitted curve.

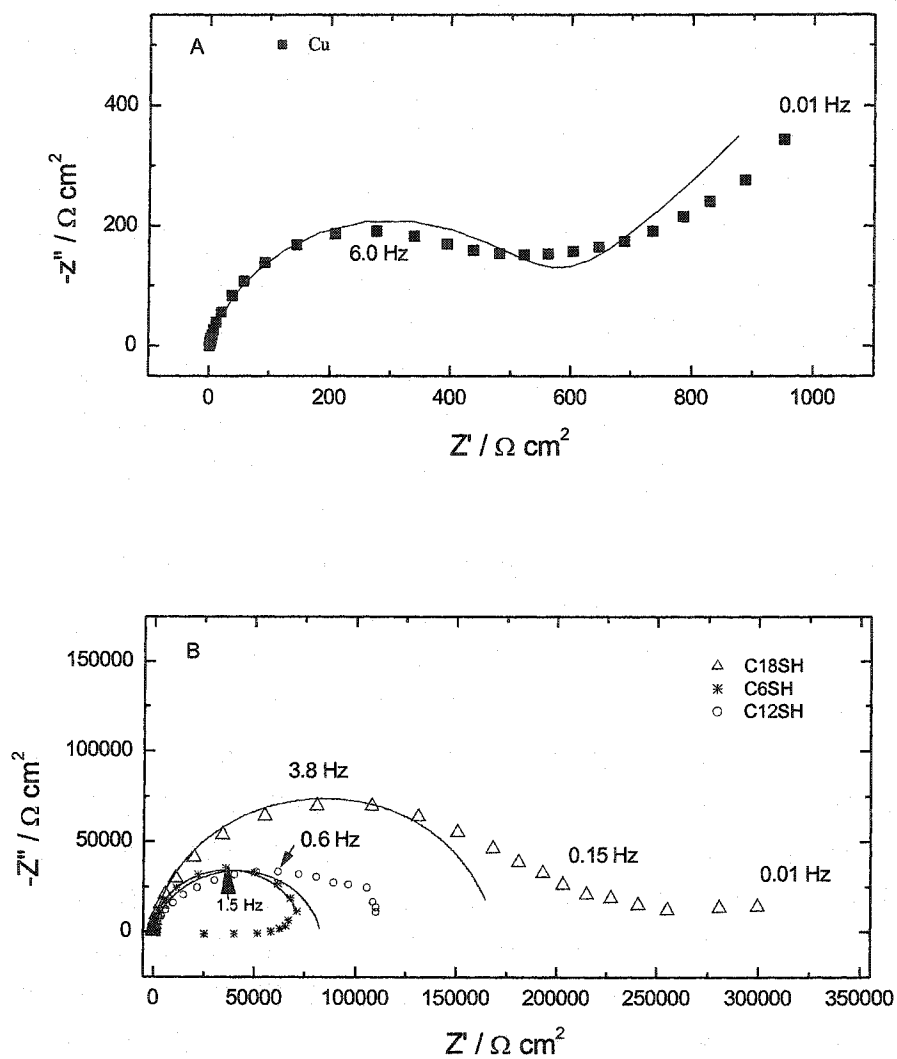
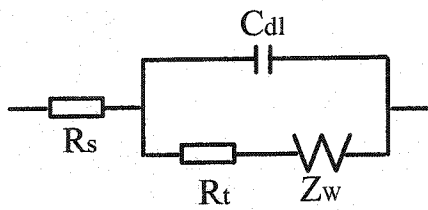
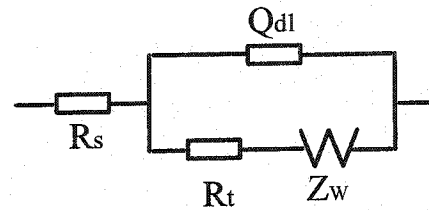


Figure 4-11. Nyquist impedance spectra for the copper electrodes of (A) and covered by alkanethiol SAMs (B) in 0.2 M H_2SO_4 solutions at the open-circuit potentials. Alkanethiol monolayers were self-assembled for 4h. Symbols: measured data; solid line: fitted curve.

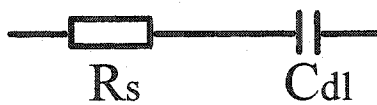


A

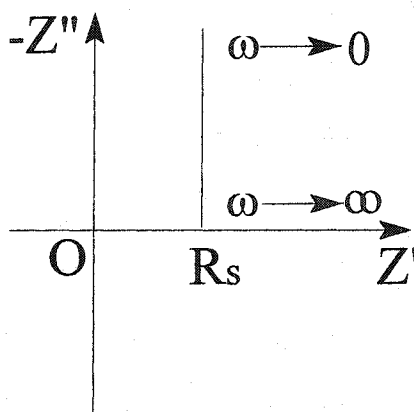


B

Figure 4-12. Equivalent circuits for the impedance spectra composed of a high frequency capacitive loop and a Warburg impedance.



A



B

Figure 4-13. The equivalent circuit of a defect-free SAM (A) and the Nyquist impedance plot for the electrode coated by the defect-free SAMs (B).

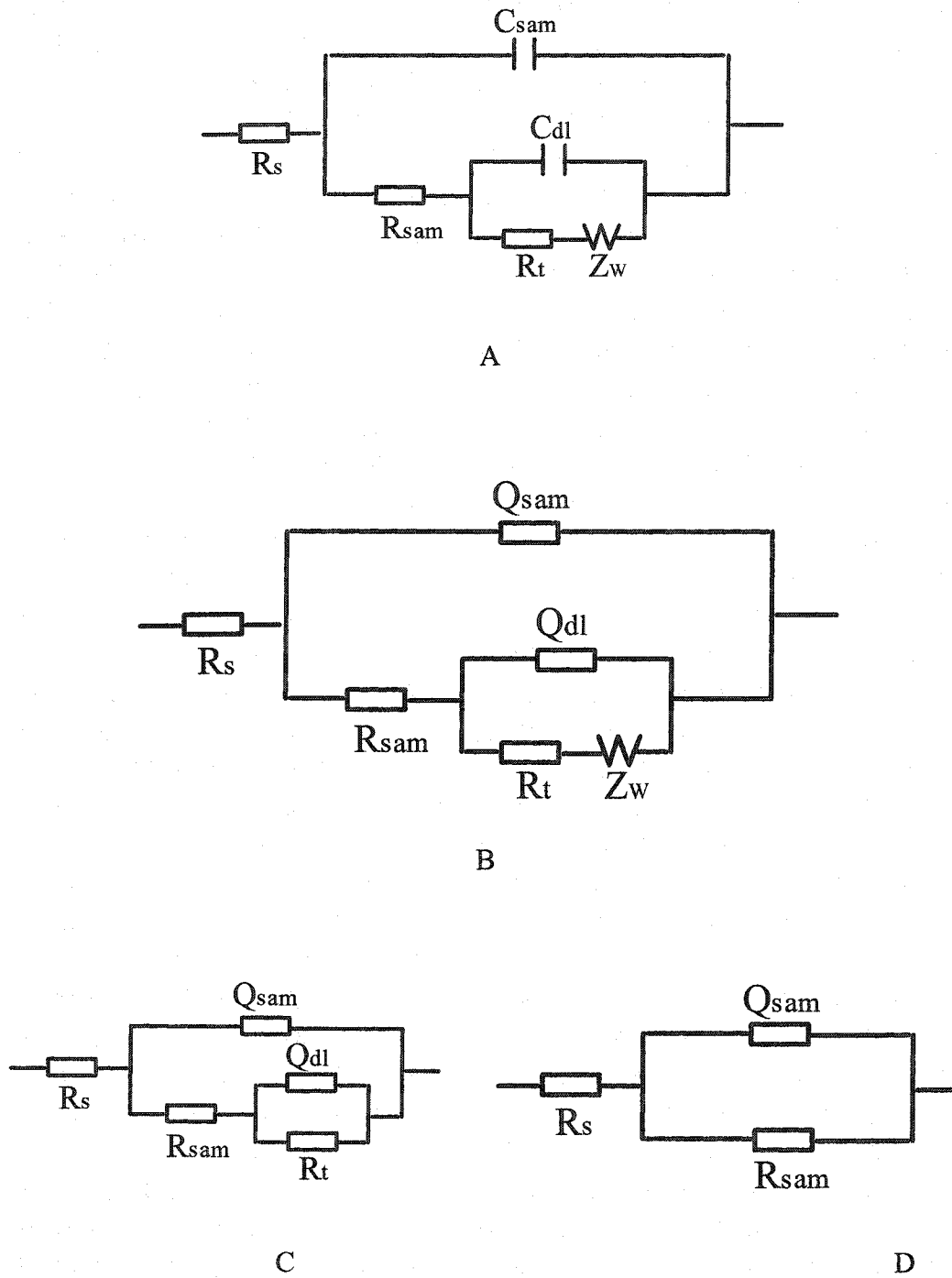


Figure 4-14. Equivalent circuits for the electrode covered by the SAMs with defects under varying conditions.

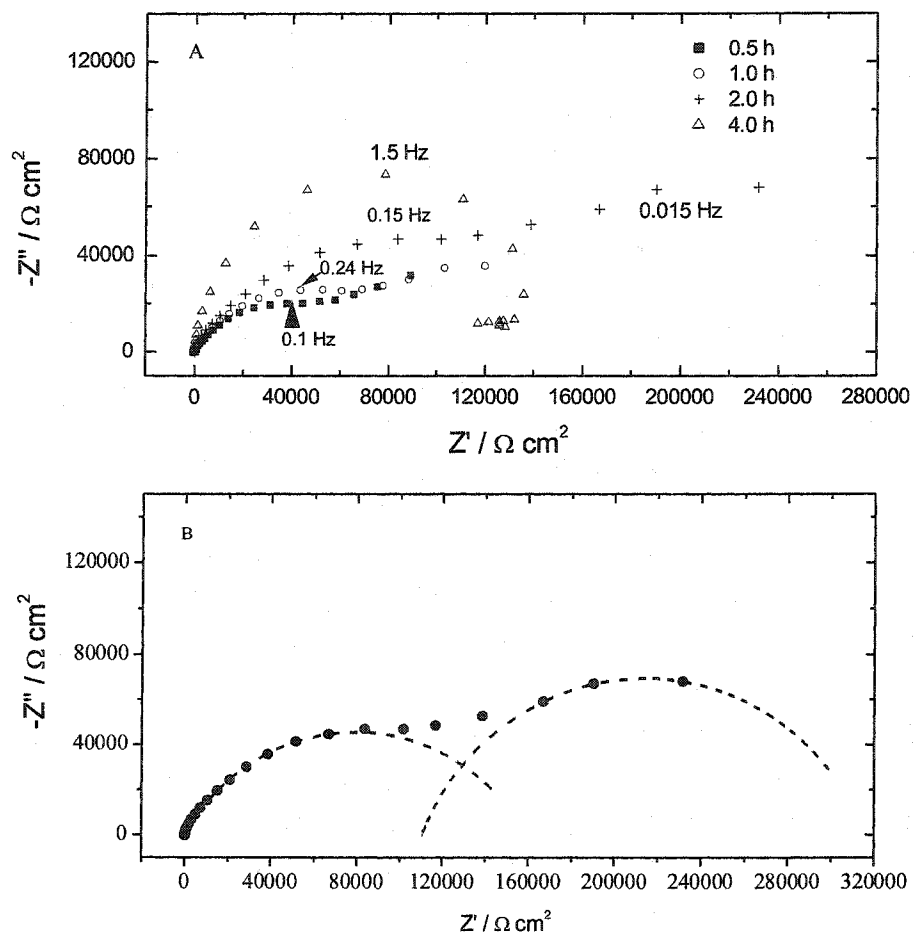


Figure 4-15. Effect of self-assembling times for C12SH SAMs at copper on their impedance behavior. Impedance measurements were carried out in 0.2 M NaCl solution at the open-circuit potentials (A) and immersion time 2h(B)

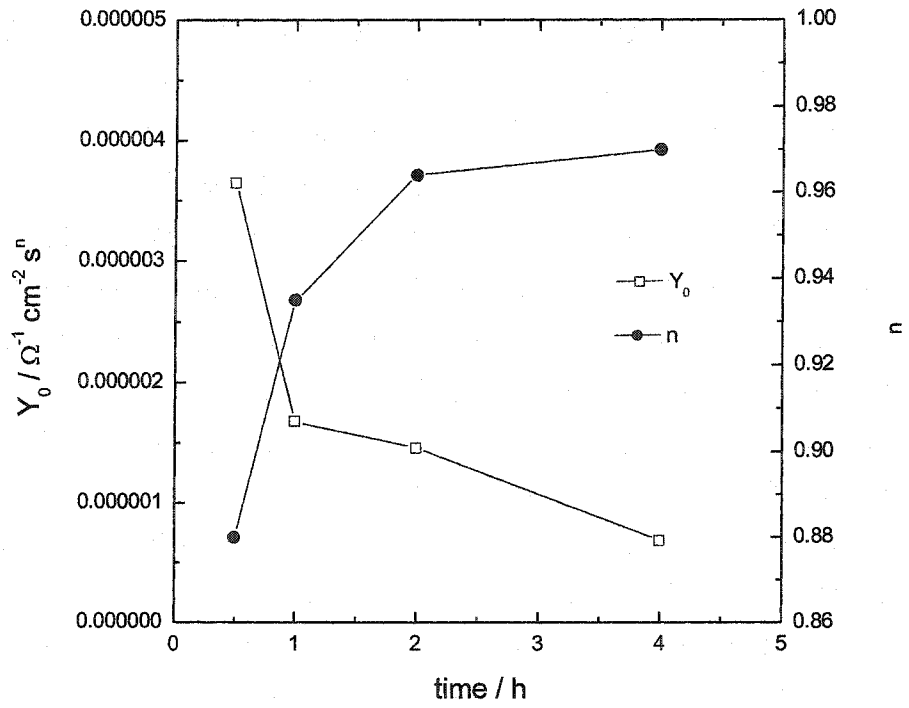


Figure 4-16. The dependence of Y_0 and n for Qsam on the formation time of C12SH SAMs.

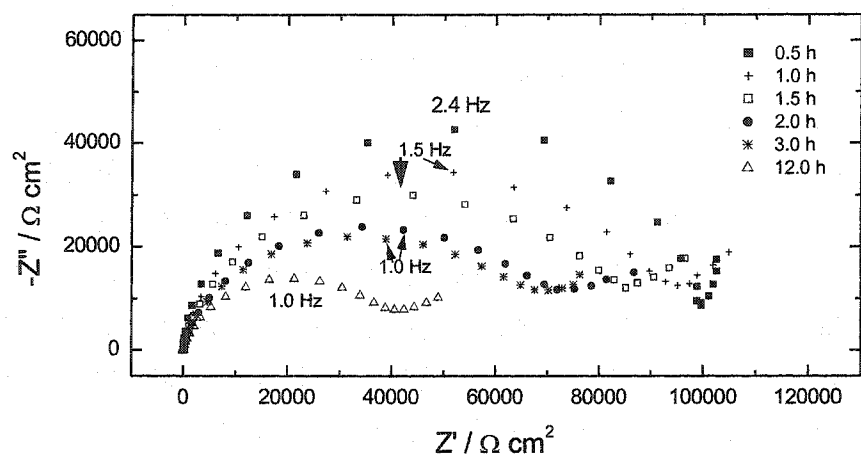


Figure 4-17. Variation of Nyquist impedance spectra with immersion time for the C12SH-SAMs-coated copper electrode in 0.2 M NaCl solution. C12SH monolayers were self-assembled in 4 h.

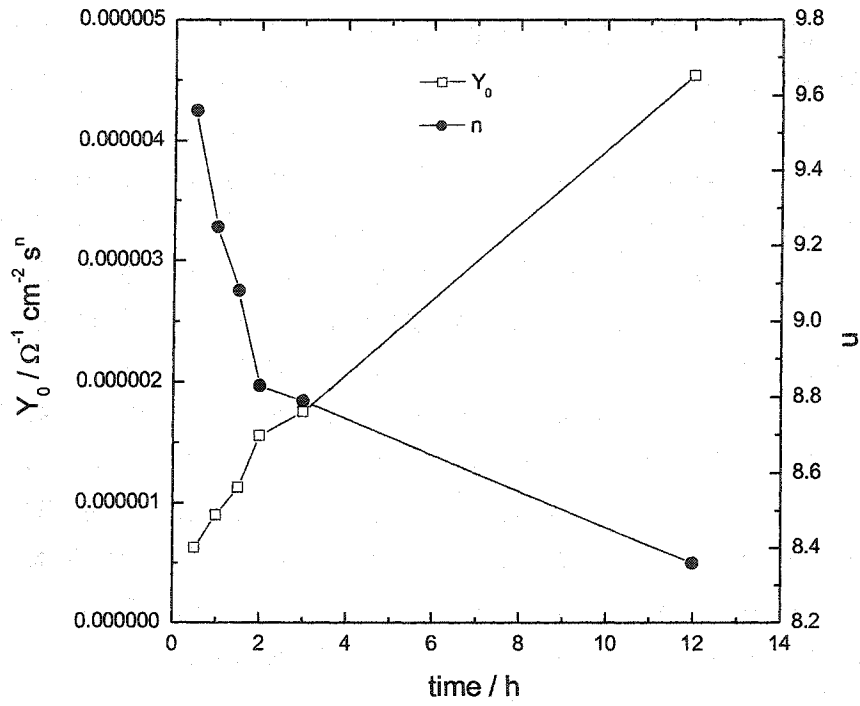


Figure 4-18. Variation of Y_0 and n for Qsam with the immersion time in 0.2 M NaCl. Before test the copper electrode was immersed in 1 mM C12SH ethanol solution for 4 h.

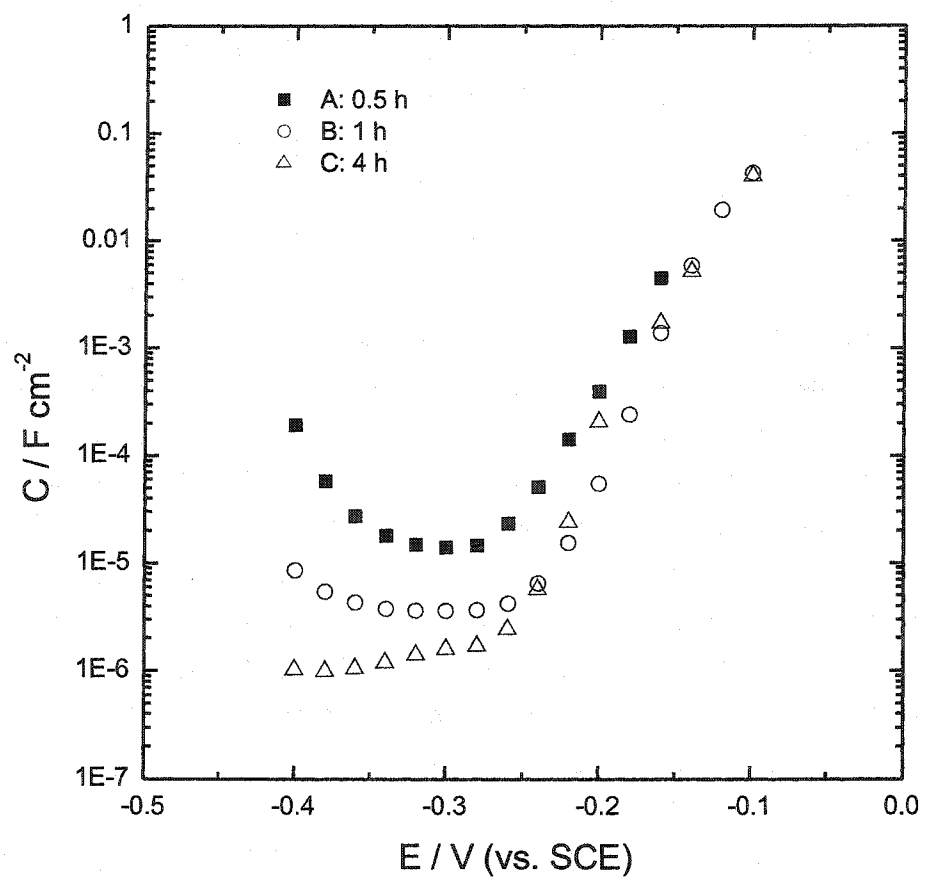


Figure 4-19. Values of capacitance as a function of applied potentials for the copper electrodes coated by the C12SH SAMs forming after various immersion times in 1 mM C12SH ethanol solution.

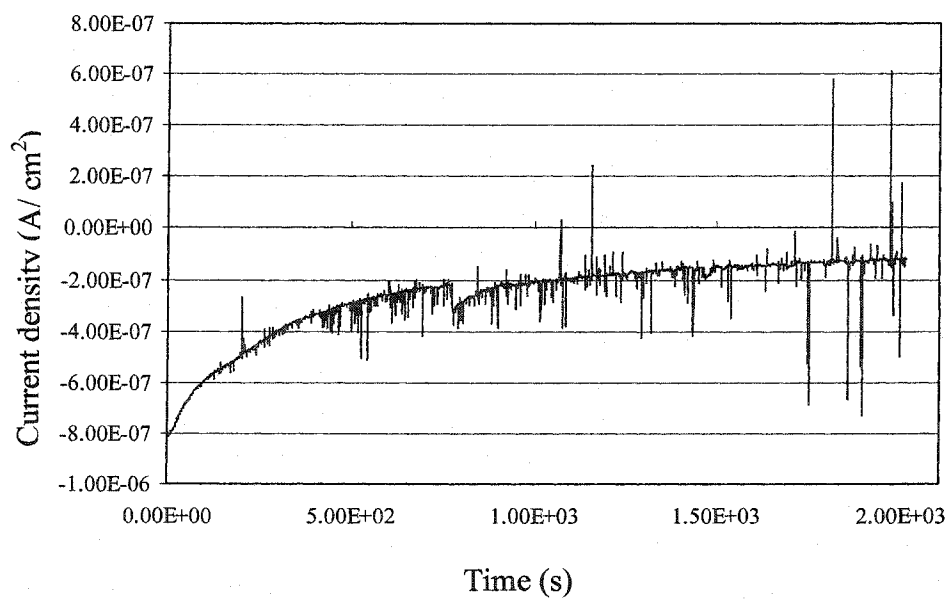
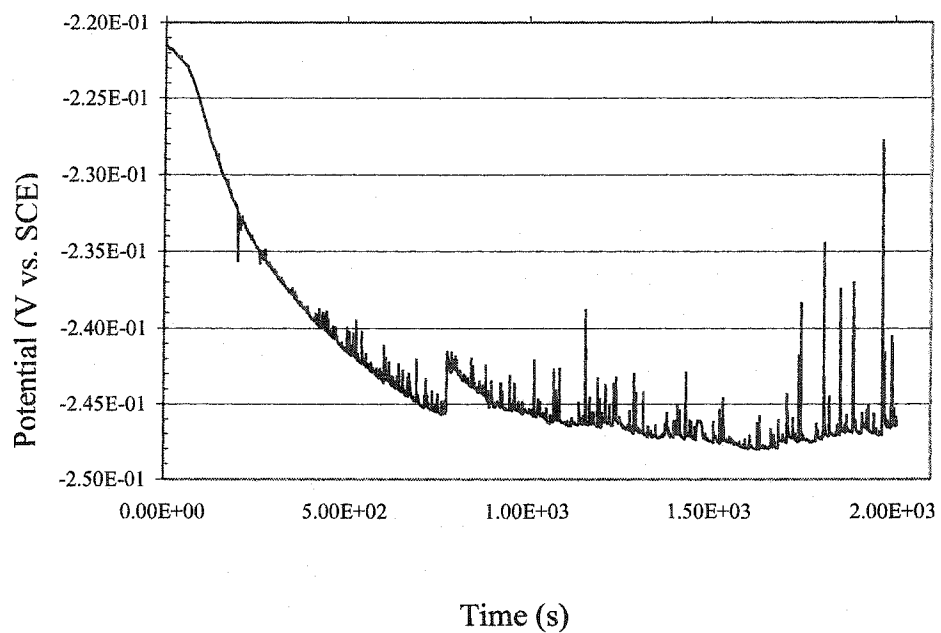


Figure 4-20. Electrochemical Noise for C18SH SAMs-covered copper electrode in 0.2 M HCl solution at the open-circuit potential (first 2000 seconds).

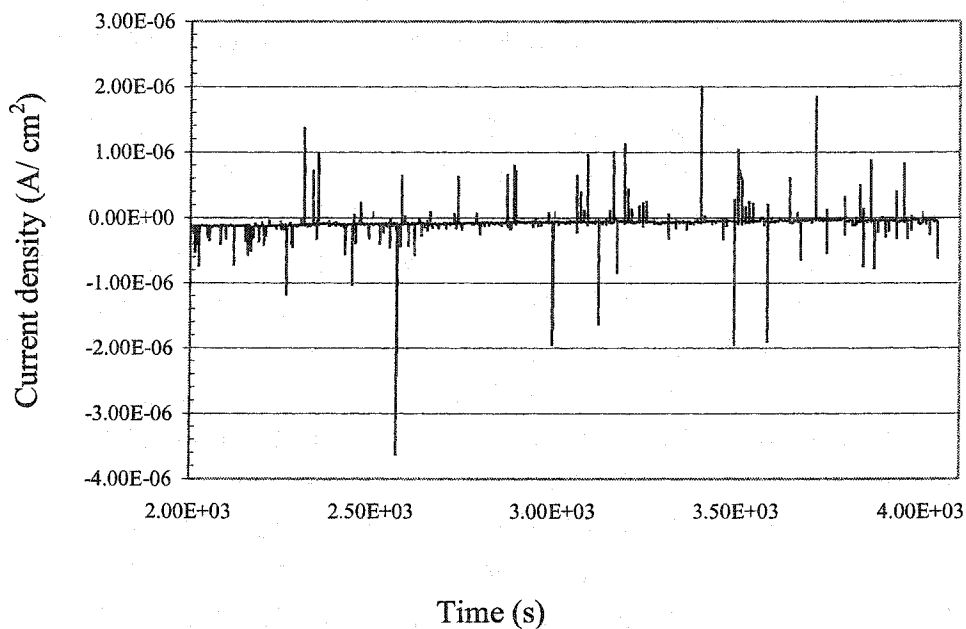
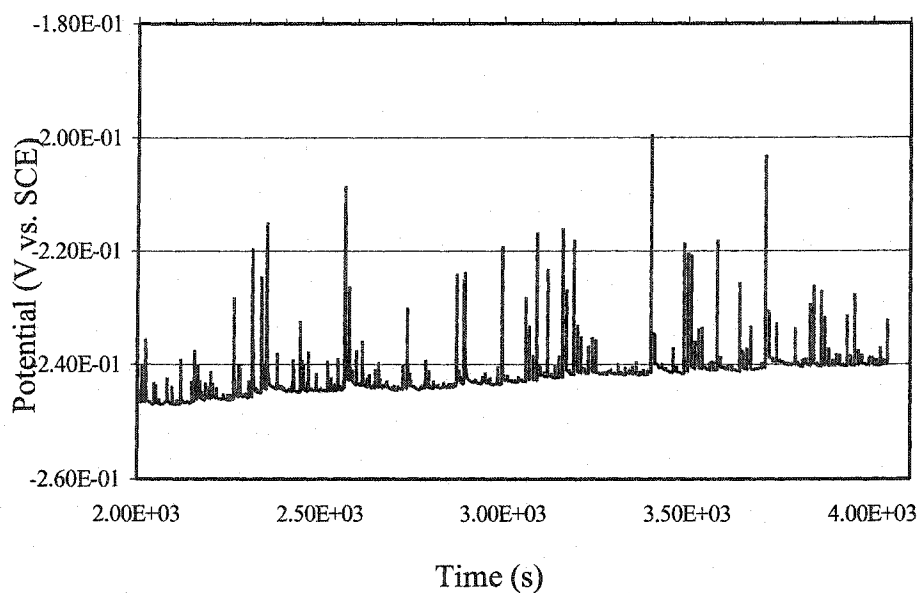


Figure 4-21. Electrochemical Noise for C18SH SAMs-covered copper electrode in 0.2 M HCl solution at the open-circuit potential (2000 – 4000 seconds)

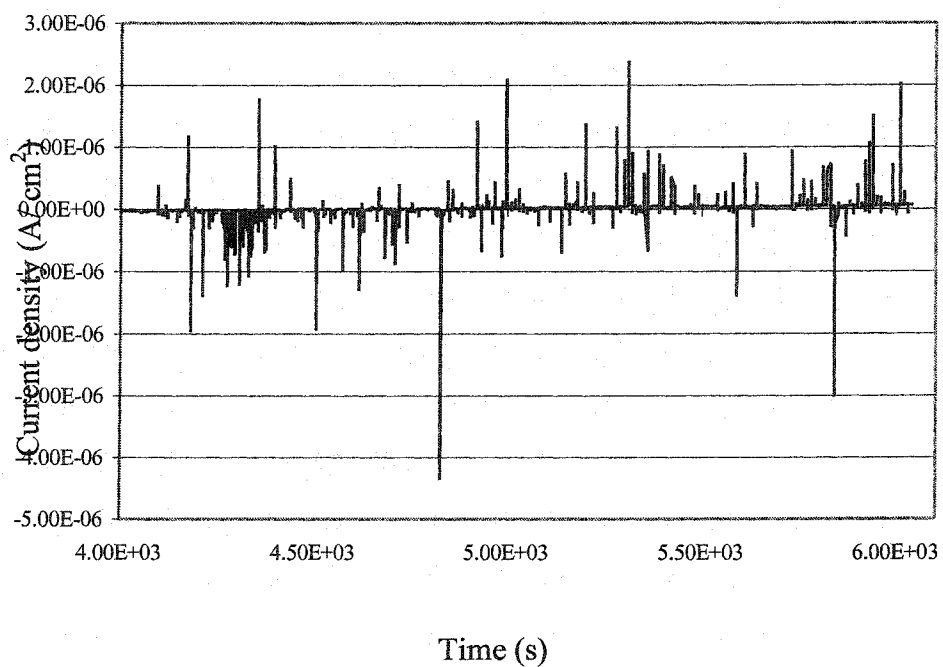
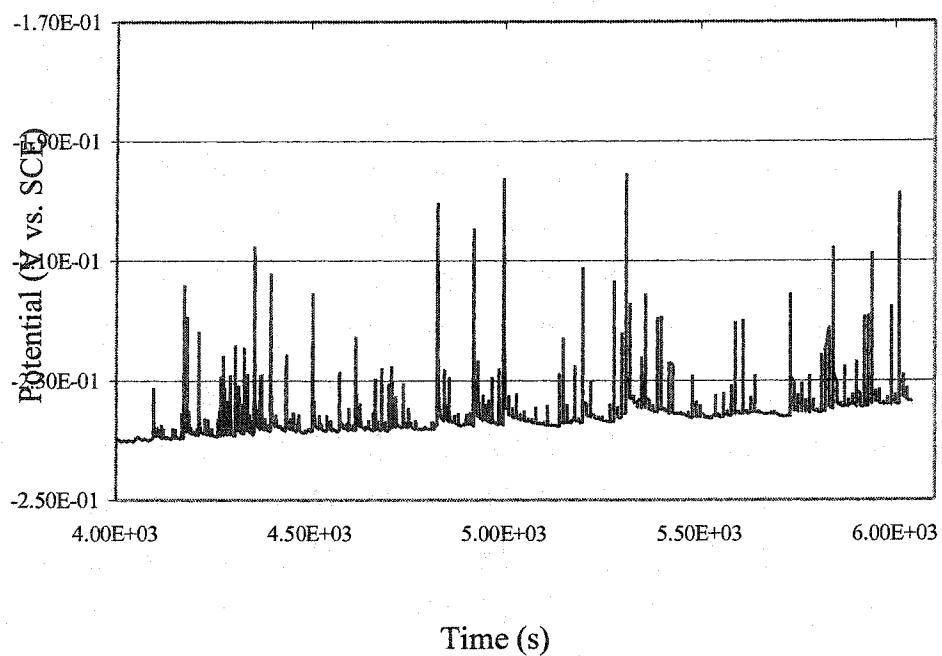


Fig 4-22. Electrochemical Noise for C18SH SAMs-covered copper electrode in 0.2 M HCl solution at the open-circuit potential (4000-6000 seconds)

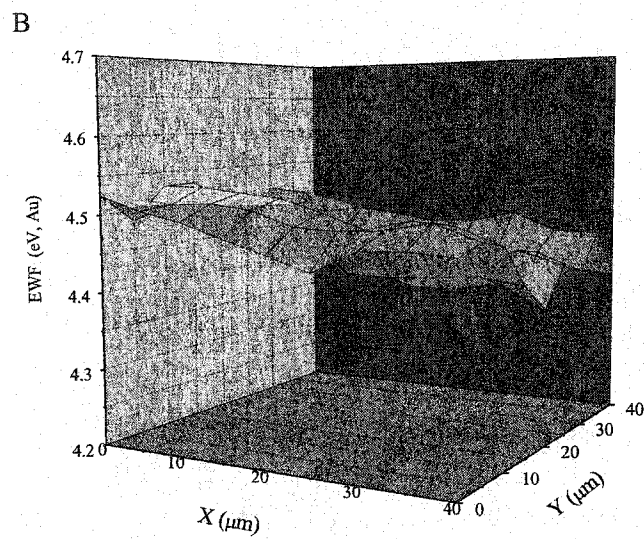
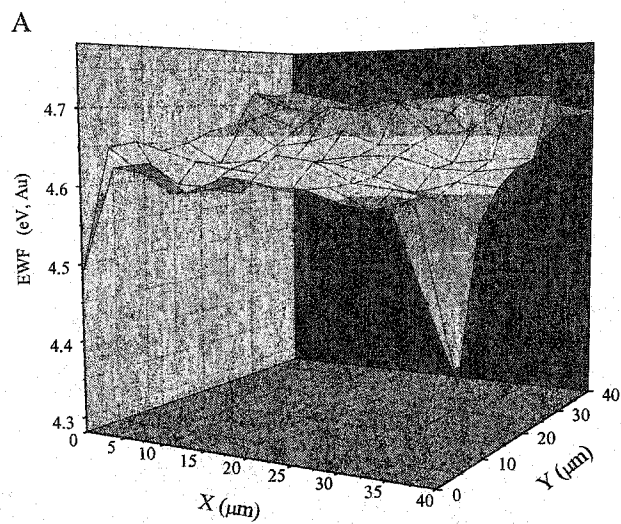


Figure 4-23. Electron work functions of copper modified by PhCH₂SH (A) and C₁₂SH (B) SAMs

CHAPTER 5. CONCLUSIONS AND FUTURE WORK

5.1. Conclusions

The self-assembled C18SH, C12SH and C6SH monolayers (SAMs) on copper provide a significant protection ability against corrosion of underlying copper in different corrosive solutions such as NaCl, HCl and H₂SO₄.

1. SAMs offers corrosion protection to copper in aqueous solution containing chloride and the corrosion protection efficiency of the SAMs on copper follows the sequence: C18SH>C12SH>C6SH.
2. Pretreatments before SAMs formation play a very important role on the quality and protection ability of SAMs. The best pretreatment was found to be cathodic reduction in 1 M HClO₄ solution, followed by etching in 7 M HNO₃ solution before self-assembly; the formed SAMs provided quite high corrosion protection efficiencies
3. SAMs will be stripped under applied potential.
4. SAMs molecules with rigid, bulk groups contain more obvious defects than those with flexible alkyl chains.
5. The mechanism or roles of SAMs in inhibiting the corrosion of copper are:
 - 1) SAMs retard the oxidation of copper from the Cu(0) to Cu(I) species.
 - 2) SAMs greatly inhibit the cathodic current of copper.
 - 3) Hydrocarbon chains can partially heal the defects by reorientation of alkanethiols around the defects.

5.2. Future work

The corrosion protection of alkyl thiol SAMs with different endgroups, such as hydroxyl, carboxyl, and amine groups, on copper should be investigated in electrolyte solutions in order to study the relationship of the corrosion protection with surface hydrophilicity.

It is also worthwhile to increase the stability of self-assembled monolayers by chemical modification and/or additional specific interchain interactions. Introducing dipole-dipole and/or hydrogen bonding interactions within the monolayers will result in the enhancement of ordering and packing in the monolayer. Alkanethiol SAMs with functional groups are of significance for chemical reaction and surface engineering.

For industry application, it is also important to investigate the self-assembled monolayers on other metal substrates such as iron and carbon steel.